Universidad de Oviedo
Universidá d'Uviéu
University of Oviedo

MASTER'S DEGREE IN ANALYTICAL AND BIOANALYTICAL SCIENCES

Master's Thesis

Bioanalytical platforms for biomarkers quantification employing doped inorganic nanoparticles

Plataformas bioanalíticas para la cuantificación de biomarcadores empleando nanopartículas inorgánicas dopadas

PABLO RODRÍGUEZ SUÁREZ

Oviedo, July 2020

INDEX

A. ABSTRACT/RESUMEN

Protein biomarker analysis is a hot topic in bioanalysis, with a high potential in diverse fields, from biomedicine, in areas such as oncology or ageing related disorders, to the pharmaceutical or food industries, among others. However, the complexity of the biological media constitutes a major barrier for these analyses which has to be overcome, as they need to pursue an excellent performance both in *in vitro* and in *in vivo* analyses. To this purpose, the use of room temperature phosphorescence (RTP) measurements, with lifetimes in the order of milliseconds, allows the avoidance of the characteristic biological fluorescence through the use of time resolved analysis, leading to clearer spectra. A powerful luminescent probe widely used in bioanalysis are Quantum Dots (QDs), crystalline semiconductor nanoparticles of only a few nanometers in diameter with special features such as fluorescence, explained in terms of the quantum confinement effects consequence of their small size. By doping the crystalline lattice of QDs with atoms of another element (d-dots), phosphorescence-like emission can be achieved, with the subsequent advantages already mentioned.

In this work, manganese doped ZnS QDs (Mn:ZnS QDs) were synthesized and used for the detection and quantification of prostate specific antigen (PSA), a protein biomarker employed for the detection of several organic disorders, such as prostate cancer. QDs were bioconjugated to antibodies, optimizing their ratio to obtain the better signal without affecting to the antibodies' recognition ability, and an immunoassay was performed, based on the antigen-antibody binding specificity. Employed QDs present a second advantage, besides their phosphorescence emission: they can be analyzed by Inductively Coupled Plasma-Mass Spectrometry (ICP-MS), an elemental technique with an extreme sensibility, able to quantify the metallic atoms present on the QDs (Zn and Mn) without any significative interferences. As the antibody-QDs ratio was controlled and known, PSA concentrations could be easily obtained, reaching limits of detection in the order of pg/mL, more than enough for prostate cancer clinical diagnosis.

El análisis de biomarcadores proteicos en un tema candente en bioanálisis, con un alto potencial en diversos campos, desde la biomedicina, en áreas como la oncología o los trastornos relacionados con la edad, hasta las industrias farmacéutica o alimentaria, entre otros. Sin embargo, la complejidad del medio biológico constituye una importante barrera para estos análisis que debe ser superada, pues estos deben mostrar un desempeño excelente tanto en análisis *in vitro* como en *in vivo*. Con este fin, el uso de fosforescencia a temperatura ambiente (RTP), con tiempos de vida en el orden de los milisegundos, permite evitar la característica fluorescencia del medio biológico mediante el uso de análisis de tiempo resuelto, consiguiendo espectros más limpios. Una importante sonda luminiscente ampliamente usada en bioanálisis son los Quantum Dots (QDs), nanopartículas cristalinas semiconductoras de tan solo unos pocos nanómetros de diámetro con características particulares como la fluorescencia, explicadas en base a los efectos del confinamiento cuántico producto de su pequeño tamaño. Dopando la red cristalina de los QDs con átomos de otro elemento (d-dots), se puede obtener una emisión fosforescente, con las consiguientes ventajas ya mencionadas.

En este trabajo, QDs de sulfuro de zinc dopados con manganeso (Mn:ZnS QDs) fueron sintetizados y empleados para la detección y cuantificación de antígeno prostático específico (PSA), un biomarcador proteico empleado para la detección de diversos trastornos orgánicos, como el cáncer de próstata. Los QDs fueron bioconjugados a anticuerpos, optimizando la proporción entre ambos para obtener la mejor señal posible sin afectar a la habilidad de reconocimiento de los anticuerpos, y se llevó a cabo un inmunoensayo en placa, basado en la especificidad de la unión antígeno-anticuerpo. Los QDs empleados presentaban una segunda ventaja, aparte de su emisión de fosforescencia: pueden ser analizados por espectrometría de masas por plasma de acoplamiento inductivo (ICP-MS), una técnica de análisis elemental con una sensibilidad extrema, capaz de cuantificar los átomos metálicos presentes en los QDs (Zn y Mn) sin ninguna interferencia significativa. Como la proporción anticuerpo-QDs fue controlada y conocida, las concentraciones de PSA pudieron ser fácilmente obtenidas, alcanzando límites de detección en el orden de los pg/mL, más que suficiente para el diagnóstico clínico del cáncer de próstata.

B. INTRODUCTION

B.1. Biomarkers

Nowadays there exist two main research areas in clinical research, early detection of diseases and development of new treatments, being the use of biomarkers widely extended for achieving the former goal. According to the Food and Drugs Administration (FDA) and the National Institute of Health (NIH) Biomarker Working Group, a biomarker is "a defined characteristic that is measured as an indicator of normal biological processes, pathogenic processes, or biological responses to an exposure or intervention, including therapeutic interventions" (*1*), although several subtypes can be identified, and therefore classified, according to their purpose. According to their nature, there exist a huge variety of biomarkers, from DNA fragments to vesicles or proteins, among others. Proteins are responsible of a huge number of biological and biochemical processes within organisms, like DNA replication or the transport of different compounds. They are produced via RNA translation at the ribosomes, so they can be regarded as the usable form of the genetic information stored on the DNA (Figure 1).

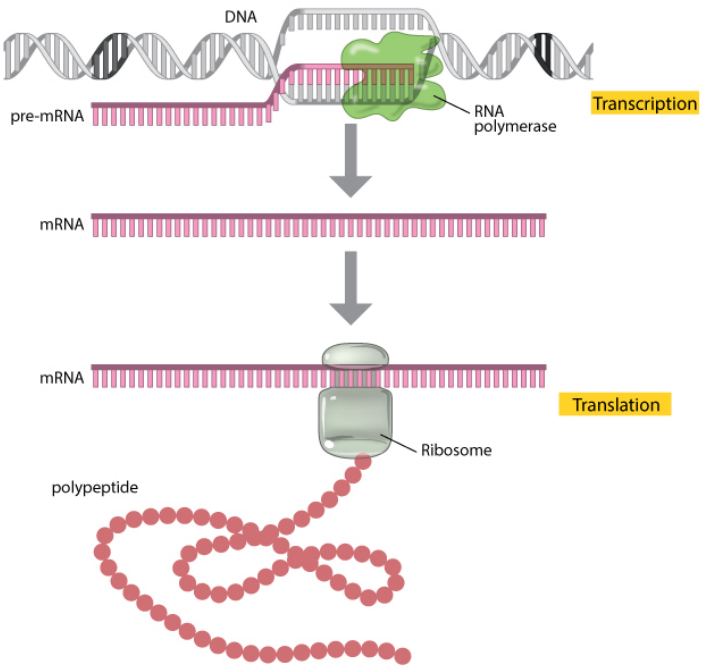

Figure 1: Scheme representing protein synthesis. Source: https://www.nature.com/scitable/topicpage/translation-dna-to-mrna-to-protein-393

The lack of expression of certain proteins in the organism (i.e. their absence) can be an indicator of abnormal state, so does their overexpression, errors during their synthesis and many other factors concerning the proteome. Moreover, in many disorders, such as in the case of tumors, a premature detection can be directly correlated to a better prognosis during the treatment, so great efforts are put into the early detection of biomarkers. For these reasons, very high sensitivity is demanded to the bioanalytical techniques employed on protein identification and quantification, so several disorders and diseases can be identified as soon as possible. However, sometimes these criteria are difficult to fulfill. When analyzing genomic biomarkers, proviso they are present in low concentrations, an amplification technique such as the polymerase chain reaction (PCR) can be employed, so extremely low limits of detection can be achieved, but direct amplification techniques when facing protein biomarkers are scarce. Analyses in biological media show an extra challenge as well: the high complexity of the biological matrix. This matrix, composed by a huge number of different biomolecules, obstructs greatly the direct analysis of a specific component of the sample by interfering with its signal, reducing the selectivity of several methodologies. For that reason, new strategies pursuing ultra-sensitive and ultra-selective analysis of proteins are being developed nowadays.

B.1.1. *Prostate specific antigen*

Prostate specific antigen (PSA) is a protein produced by the prostate glandule, usually employed as biomarker for the diagnosis of prostatic cancer, the cancer with the highest prevalence among men. According to the American Cancer Society, PSA concentrations between 4 and 10 ng/mL of blood indicate a 25% probability of having prostatic cancer, while values over 10 ng/mL raises the probability up to 50% (*2*). As women do not have prostate, it would be expected to find a zero-value PSA concentration in female serum, but this has been proved wrong. Originated in female breasts, PSA levels in women serum are at much lower concentrations than in male serum (*3*), so even recent techniques with limits of detection in the order of 0.001 ng/mL (*4*) can confront problems when facing female samples, where abnormal PSA values can also be correlated with several pathologies, such as breast cancer (*5*). Even if available techniques can fulfill the sensibility requirements demanded for the analysis of male samples, a further effort has

to be put into the development of new strategies able to analyze female samples with sufficiently low limits of detection.

B.2. Platforms and techniques used for biomarker analysis

B.2.1. *Mass spectrometry-based techniques*

Protein analysis is commonly carried out using mass spectrometry (MS) techniques, due to their better performance compared with other methodologies (*6*). MS working principle consists on the ionization and separation of molecules, or fragments of molecules, according to their mass-to-charge ratio (m/z), due to an electromagnetic field. When hitting an appropriate detector, these ionized species produce an electric signal that can be measured, and a mass spectrum showing the signal abundance as a function of the m/z of each ion is obtained. One of the main advantages of MS is the versatility that provides the selection of the ionization source, which can be chosen according to the physical state of the analyte, its size or the information pursued. For protein analysis, the most common ionization sources employed are electrospray (ESI), matrix-assisted laser desorption/ionization (MALDI) and, more recently, inductively coupled plasma (ICP), as they show a high sample throughput when facing macromolecules (*7*). ESI and MALDI produce the molecular ionization of the analyte so there will be virtually no fragmentation whatsoever, which combined with the high molecular weight range of both techniques turns them into very powerful options for the analysis of proteins and other macromolecules. While ESI requires the analyte to be in solution, so it is a suitable method to analyze proteins present in biological fluids (*8*), MALDI is based on the desorption of the material from a solid surface after the application of a laser pulse, hence it can work as a tissue imaging technique (*9*). On the other hand, ICP ionization atomizes the analyte, so no structural information can be achieved. Protein analysis by ICP-MS consists on the measurement of heteroatoms present in the molecule, however, as most of the usual atoms contained on the amino acid sequence of the protein (C, N, O, H) cannot be detected with this technique (*10*). Even though the four major elements cannot be directly measured with ICP-MS, there are elements, metals or semimetals such as Se, or no-metals such as S or P, naturally present in proteins whose quantitative measure can be used for the absolute direct quantification of proteins and peptides. Of course, complete species isolation is required, as ICP-MS does not distinguish between elemental signals

coming from different co-eluting species. To achieve such protein determination, the corresponding stoichiometry element:protein is required as well (*11*). These heteroatoms can be naturally present on the molecule or they can be introduced as tags (*12*). In Table 1 some approaches have been also developed to achieve absolute quantification of proteins using MS, existing a considerable number of methodologies available for their analysis.

Table 1: Mass spectrometry (MS) techniques for the analysis of proteins

Method	Quantification	Working principle	Ref.
SILAC	Differential	Cell cultures fed with isotopically enriched amino acids	(*13*)
ICAT	Differential	Isotopically enriched tags bonded to Cys residues	(*14*)
Enzymatic labelling	Differential	Enzymatic digestion leading to isotopically labelled peptides	(*15*)
AQUA	Absolute	Synthetic, isotopically labelled, tryptic peptides of interest	(*16*)
S/MRM	Absolute	Parent ion selected in a MS, then fragmented and one (SRM) or several (MRM) product ions analyzed in a second MS	(*17*)
ICP-MS	Absolute	Species-specific or species-unspecific isotopic dilution analysis of a heteroatom present in the protein of interest	(*18*) (*19*)

SILAC: Stable Isotope Labelling by Amino acid in Cell culture; ICAT: Isotope-Coded Affinity Tag; AQUA: Absolute QUAntification; S/MRM: Single/Multiple Reaction Monitoring; ICP-MS: Inductively Coupled Plasma-Mass Spectrometry

B.2.2. *Optical-based techniques*

However, in some occasions MS is not the best alternative regarding protein quantification. The required equipment is expensive and not every laboratory can afford it, plus its usage needs highly trained personnel. Another suitable option for protein analysis, which additionally requires cheaper and simpler equipment, are optical methods. Many proteins absorb light both in the near ultraviolet (280 nm) and in the far ultraviolet (≈190 nm) regions (*20*). By radiating a certain sample at those wavelengths, its total protein content can be estimated by measuring emission intensity. However, this method does not discern among different proteins, being only useful to quantify the total protein concentration of a sample. To quantify a specific protein, it is necessary to label it using a specific tag, so only the emission of the labelled protein will be recorded, or at least it can be discerned from the emission of other proteins. This requires a high specificity of

the tag towards the target protein, which can be achieved, among other methodologies, by using antibodies.

Other optical methodologies for protein quantification are based on the emission of photoluminescent radiation. Two distinct photoluminescent mechanisms can be defined, based on their radiative processes: fluorescence and phosphorescence. Processes involved in molecular photoluminescence are shown in Figure 2 (*21*). Molecular absorption of photons in the UV-vis range causes the electronic transition from a lower energy level of the ground electronic singlet state (S_0) to an excited state (S_1).

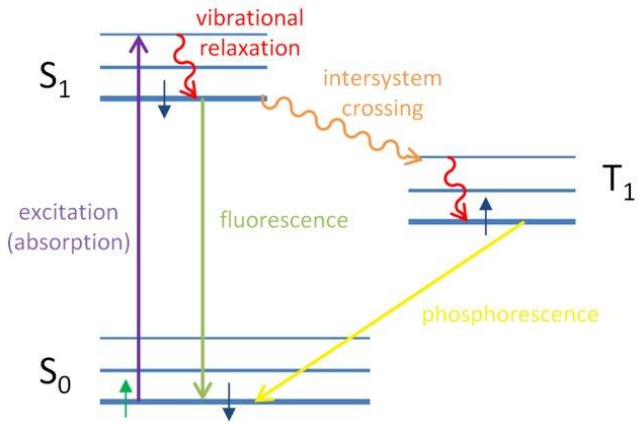

Figure 2: Jablonski diagram *(Eck, 2014)*

Once the irradiation of the molecule ceases, it will tend to go back to its ground state by losing the extra energy through different paths. Excited molecules on S_1 will lose some of their energy due to inter-molecular collisions, a process called vibrational relaxation, ending up on the lowest energetic orbital of S_1. At this point, a mayor part of the molecules will return to their ground state S_0, releasing their energy excess as photons. This process, called fluorescence, is very fast, as the transition $S_1 \rightarrow S_0$ is allowed by quantum mechanics. However, some molecules located on S_1, will not fall back directly to S_0, but they will suffer an intersystem crossing to a triplet, less energetic state, T_1. $T_1 \rightarrow S_0$ transition, which receives the name of phosphorescence, is forbidden in terms of quantum mechanics, so its probability is rather low. For that reason, phosphorescence lifetimes are significantly higher, up to the milliseconds order, than the ones observed in fluorescence, which are typically in the nanoseconds scale. As stated before, just a small number of molecules will suffer that intersystem crossing, so it comes as no surprise that

phosphorescence intensities are usually lower than fluorescence ones, unless that crossing is somehow enhanced.

One way to do this is by deoxygenating the medium, usually using sulfites. Dissolved oxygen can act as a phosphorescence quencher by means of an energy transfer, reducing phosphorescence intensity of the analyte. Another way is to introduce heavy atoms into the molecule or into the environment as iodide, which enhance the intersystem crossing, increasing the population on the triplet excited state. The last option is to reduce the collisional deactivation, which produces a non-radiative relaxation. Traditionally, this has been achieved by reducing the temperature using liquid nitrogen. but more recently, aiming to work at room temperature, new methodologies have been developed. They are based on the stabilization of molecules using a rigid medium, as micelles or solid surfaces, so intermolecular collisions are reduced, avoiding deactivation.

In Figure 2 it can also be observed how the emission energy is smaller than the excitation one, both in fluorescence and in phosphorescence processes. Consequently, emission wavelengths will be usually higher than excitation ones, unless two or more photons are absorbed simultaneously by the molecule, a process known as upconversion. The wavelength difference between excitation and emission radiation is called Stokes shift and it is more noticeable in phosphorescence than in fluorescence, as it is depicted in Figure 3.

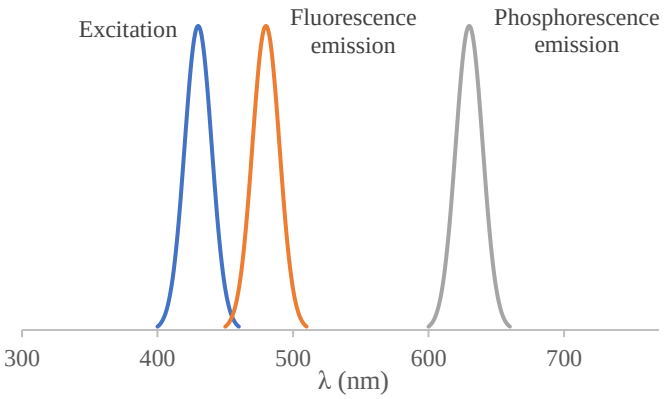

Figure 3: Stokes shift in fluorescence and phosphorescence processes

B.3. Immunoassays

Antibodies (Ab) are glycoproteins produced by living beings as a response to the presence of an unknown substance in the organism, called antigen, for which they show specificity. Although there exist many types, the most common antibody employed in bioanalysis is immunoglobulin G (IgG), whose protein part is showed in Figure 4. It is formed by four chains, two heavy (H) ones and two light (L) ones, forming a "Y" structure, which can be divided into an antigen-binding fragment (Fab) and a crystallizable fragment (Fc). Each chain presents several constant parts (CH and CL for heavy and light chains, respectively) and a variable part (VH and VL for heavy and light chains, respectively), which interact with antigens through the complementarity determine regions (CDR). The set of CDRs of an antibody are called paratopes, and they present a strong affinity towards the antigenic determinant regions of the antigen, called epitopes. The structural conformation of the Ab has to be taken into account by the time of performing their bioconjugation to the tag, so the final disposition of the antibody leaves its paratopes orientated towards the antigen, which in this case is the target protein.

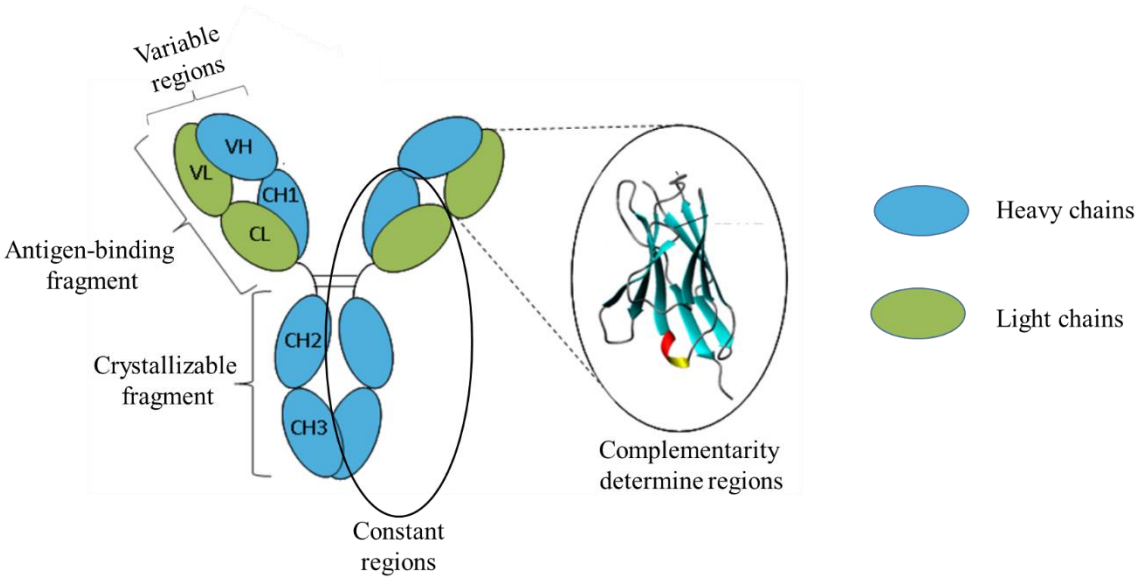

Figure 4: Immunoglobulin G (IgG) general structure. Adapted from: https://absoluteantibody.com/antibody-resources/antibody-overview/antibody-structure/

This constitutes the working principle of immunoassays, in which the target analyte is recognized, and therefore bonded, to its specific antibody. The conjugate Ag:Ab can be subsequently detected by different methodologies, as it will be discussed in B.3.1 section. In addition, due to the high specificity of this binding, immunoassays present both great

sensitivity and selectivity parameters, reaching low limits of detection, so they constitute a powerful tool in bioanalysis.

B.3.1. *Immunoassays classification*

B.3.1.1. Types of immunoassays according to their format

As depicted in Figure 5, immunoassay structures can vary significantly, existing a broad range of possibilities to choose from by the time of designing the assay.

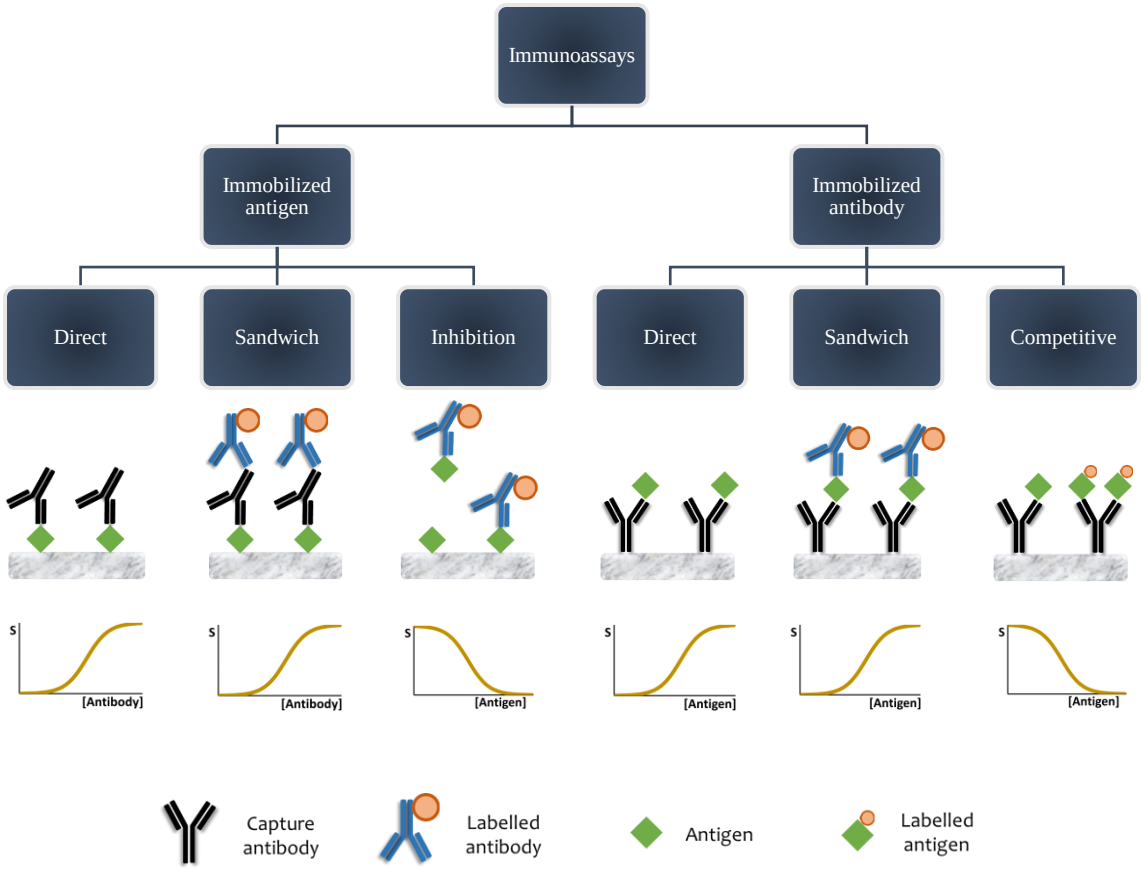

Figure 5: Immunoassays classification according to their format

In this work, an antibody immobilized sandwich immunoassay, which besides is the most common immunoassay format, will be performed, so it will be explained in further detail. In antibody immobilized sandwich immunoassays, a capture antibody, specific for the target analyte, is attached to a solid surface, such as an ELISA well-plate. Once the antigen is present in the form of standards or in a real sample, it binds to antibodies due

to the paratopes-epitopes interaction. As several antibodies can bind to the same antigen through its different epitopes, a labelled antibody can be introduced into the conjugate, forming the so called "sandwich" capture Ab – Ag – labelled Ab, and explaining why an increasing signal is expected as the antigen concentration increases.

B.3.1.2. Types of immunoassays according to the detection method

Immunoassays have come a long way since the first one was designed on 1959 by Yalow and Berson (*22*). On their work, they used antibodies to detect insulin using a radiative probe as tag, so radioimmunoassays (RIA) can be considered as the first type of immunoassays. However, the risk associated to using radiative isotopes fostered the development of safer options, such as counting immunoassays (CIA). The tag in CIA are polymer beads attached to the antibody, which can be analyzed by optical methods. If the antibody specific analyte is present in the sample, an accumulation of beads will be produced around it and just a few non-bonded beads will remain in solution. Both agglomerated or free beads can be counted and related to the concentration of analyte in the sample, by means of an easy and cheap analysis (*23*). Another possibility is the use of enzymes as tags, receiving the name of enzyme-immunoassay (EIA) or the well-known enzyme-linked immunosorbent assay (ELISA). The working principle of both techniques is the same (*24*): when the analyte is present in the sample, antibodies are linked to it. These antibodies are then detected by secondary antibodies, labelled with a certain enzyme. Finally, the substrate of the enzyme is added, so if the analyte was present on the sample a physical change, such as a color variation, will be observed, due to the catalytic conversion of the substrate by the enzyme. Other immunoassays based on colorimetric measurements are chemiluminescence immunoassays (CLIA), which use a certain molecule as tag which emits light in the presence of another reagent, which fulfills the same function that the substrate in EIA or ELISA. So, in this case, light is produced through a chemical reaction. In the last type of immunoassays, emission of light is triggered by the radiation of the tag using electromagnetic waves of a specific wavelength, characteristic for each molecule. This is the case of fluorescence immunoassays (FIA), which use a fluorescent probe as tag, whose nature has extensively changed along the years. In Table 2 are summarized the most widely used immunoassays, as well as their main features.

Table 2: Immunoassays classification regarding their detection

Immunoassay	Tag	Detection	Trigger
RIA	Radioisotope	Optical	Automatic
CIA	Polymer beads	Optical, mass spectrometry	None
EIA/ELISA	Enzyme	Optical, electrochemical	Enzyme substrate
CLIA	A reagent of the luminescent reaction	Optical	The other reagent of the luminescent reaction
FIA	Luminescent molecule	Optical	Electromagnetic radiation of a specific wavelength

RIA: Radio ImmunoAssay; CIA: Counting ImmunoAssay; EIA: Enzyme ImmunoAssay; ELISA: Enzyme-Linked ImmunoSorbent Assay; CLIA: ChemiLuminiscence ImmunoAssay; FIA: Fluorescence ImmunoAssay

B.4. Nanotechnology

B.4.1. *Definition and analytical applications*

Nanotechnology development gave rise to a whole new series of probes, among which are metal nanoparticles. The definition of nanomaterial is a controversial subject, which varies depending on the legislation (*25*). According to the European Commission, a nanomaterial can be regarded as any "natural, incidental or manufactured material containing particles, in an unbound state or as an aggregate or as an agglomerate and where, for 50% or more of the particles in the number size distribution, one or more external dimensions are in the size range 1 nm - 100 nm" (*26*), so metal nanoparticles can be therefore regarded as clusters of atoms of the same metal whose dimensions are comprised in the nanoscale. Nanoparticles can be used as probes for a CIA, but due to their small size, they also present some particular physicochemical properties (*27*), being their optical activity the most interesting one from the point of view of this work. For instance, gold nanoparticles present a size-dependent emission, produced by the effect of the surface plasmon resonance (SPR) and which can be used for the colorimetric detection of analytes. By reducing more the size of the particles, metal nanoclusters (NC) are obtained, containing just some tens of metal atoms and presenting some extra interesting features compared to nanoparticles, like two-photon absorption (*28*). Nanowires are another example of nanodevices, this time having only one dimension outside the nanoscale. They are excellent electrical conductors due to quantum confinement effects,

opening the door to some innovative applications, such as fluorescence amplification (*29*).

B.4.2. *Quantum Dots (QD)*

However, one of the most extended probes in bioanalysis, and the one employed in this work, are Quantum Dots (QDs). QDs are semiconductor nanocrystals with all their dimensions in the nanoscale, developed in 1981 for Alexei Ekimov (*30*). They are formed by elements from the II-VI, III-V, IV-VI groups of the periodic table, and their general structure can be divided into a core, a shell, and a coating, as depicted in Figure 6. The core presents tunable luminescent properties, which can be explained in terms of the quantum confinement effects produced by its nanoscopic size (*31*). However, the light emitted by the core is not continuous, due to a phenomenon called blinking, and it suffers photobleaching, losing its activity after some time. By surrounding the core with a shell, usually made of ZnS, blinking is avoided, obtaining a continuum emission. To solve photobleaching, QDs must be covered with a polymeric coating, which avoids their degradation and also prevents QDs aggregation. In addition, this external layer protects organisms against the inherent toxicity of QDs and it can be functionalized, achieving a high specificity towards the desired analyte (*32*).

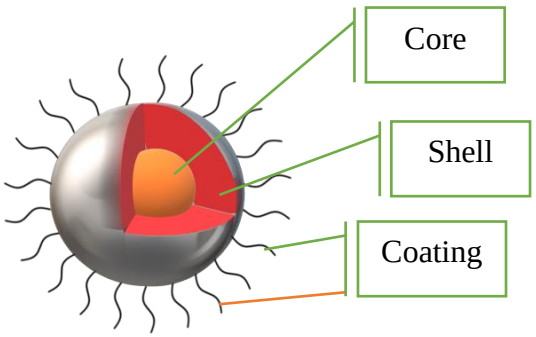

Figure 6: General Quantum Dot structure

B.4.2.1. Synthesis of Quantum Dots

Many methodologies have been developed to synthesize QDs, although all of them can be classified into two main groups, top-down and bottom-up procedures. Top-down synthesis is based on the lithography of bulk semiconductor materials, using for instance laser ablation (*33*), until nanoparticles are obtained. On the other hand, bottom-up synthesis is performed by mixing the required reagents, which vary depending on the composition of the QD, so nanoparticles formation is induced. In bottom-up approaches, QDs coating can be performed simultaneously to their synthesis, whereas in top-down synthesis, coating requires an additional step. In bottom-up procedures, it is common to stabilize QDs with hydrophobic ligands, such as Cysteine or dihydrolipoic acid (DHLA). This can hinder some of their applications, as the ones involving biological media. In those cases, hydrophobic ligands can be exchanged by hydrophilic ones or the whole QD can be encapsulated within a hydrophilic polymer (*34*).

B.4.2.2. Quantum Dots properties

QDs are more stable than traditional fluorophores, but they present another great advantage: their tunable properties. By modifying QDs size, shape or composition, their optoelectrical properties can be adjusted, which combined with their narrow emission spectrum, opens the door to, for instance, multiplexing analyses (*35*). In fact, by doping QDs core (d-dots), it is possible to modify their radiative process and therefore their luminescence properties. As an example, ZnS QDs present intrinsic fluorescent emission, but if their core is doped with Mn^{2+} atoms their luminescence lifetime increases up to several milliseconds, matching the typical phosphorescence emission features (*36*). Mn:ZnS QDs are excited at the ZnS QDs absorption wavelength (300 nm) and an energy transfer to the Mn^{2+} electronic states occurs shortly afterwards (*37*). The explanation for their long decay times resides in the d-d spin forbidden transition of Mn, $^4T_1$-$^6A_1$ (*38*), which produces a delay in the luminescence emission with respect to the one of ZnS QD and a small emission wavelength shift. This phenomenon opens the door to a wide range of applications, as it will be discussed in B.4.2.4 section.

B.4.2.3. Characterization of Quantum Dots

Due to all the factors affecting QDs emission (size, shape, composition…), it is crucial to perform an exhaustive characterization after their synthesis, to assure that the optical properties obtained match the ones desired. Apart for luminescence measurements, which can proportionate information about QDs concentration (which is directly related to the intensity recorded) or composition (by observing their excitation and emission wavelengths), several analytical techniques can be used with this purpose, such as X-ray diffraction (XRD) or transmission electron microscopy (TEM), which provide a huge amount of information, concerning morphology, crystallography and composition of the nanoparticles; dynamic light scattering (DLS), which allows the determination of the hydrodynamic radius of QDs and of their size distribution based on differences in diffusion rates caused by their Brownian motion; or multiangle light scattering (MALS), that provides information about the molecular weight of the particle by measuring the scattered light at different angles. Among all of these, there exist two extremely powerful and complementary techniques for the characterization of QDs: inductively coupled plasma-mass spectrometry (ICP-MS) and asymmetrical flow field-flow fractionation (AF4). ICP-MS can be used in order to record the elemental composition of QDs or to measure QDs concentration on a sample (*39*). ICP-MS provides a multi-elemental analysis with a high sensitivity for almost all elements in the periodic table, so it is possible to know the elements present and their concentration on a certain sample. Furthermore, by performing a single particle ICP-MS (spICP-MS, *40*), QDs concentration and even the mass of each nanoparticle can be obtained. From these data, individual QDs mass or even size can be calculated (*41*). However, QDs must be separated before entering the ICP-MS, so the data obtained can be assigned to a specific QD type. AF4 has shown a high potential as a separation technique regarding QDs, allowing their separation as a function of their size and coating. In addition, it can be easily coupled to ICP-MS, so it became one of the best options available, providing highly valuable quantitative information about the particles. Together, AF4 and ICP-MS are an excellent option for the separation, identification, characterization, and quantification of QDs.

B.4.2.4. Applications of Quantum Dots in bioanalysis

QDs present a wide variety of applications, most of them regarding bioimaging. Due to the possibility of obtaining a phosphorescence like emission through d-dots, typical biological media fluorescence can be avoided performing a time-resolved analysis, so only labelled structures will be visible. As their toxicity is greatly reduced thanks to their polymeric coating, QDs are suitable for *in vivo* studies (*42*), so they can be used as diagnosis tools in biomedical studies. Other Quantum Dots applications in bioanalysis are summarized in Table 3.

Table 3: Quantum Dots applications in bioanalysis

Application	Ref.
Chemical sensing for the detection of metals	(*43*)
Catalytic structure	(*44*)
Toxins detection	(*45*)
FRET donors	(*46*)

FRET: Förster Resonance Energy Transfer

B.4.2.5. Quantum Dots bioconjugation to antibodies

There exist many methodologies to bioconjugate QDs to antibodies. However, as it has been already said, antibody orientation is a key parameter in immunoassays, so the bioconjugation technique employed needs to leave the paratopes oriented towards the antigen, ideally in an end-on position. Antibody bioconjugation techniques can be classified according to the nature of the interaction, which can be physical, covalent, or based on affinity. Physical interactions, like adsorption, do not implicate the formation of chemical bonds between the antibody and the QD, leading therefore to low stabilities and a non-oriented disposition, so their application is limited. Covalent interactions are based on the formation of chemical bonds between functional groups of the antibody and of the QD. As it is shown in Figure 7, antibodies have several different functional groups all over their structure, so the orientation of the antibody will depend on which group is made to react with the QD.

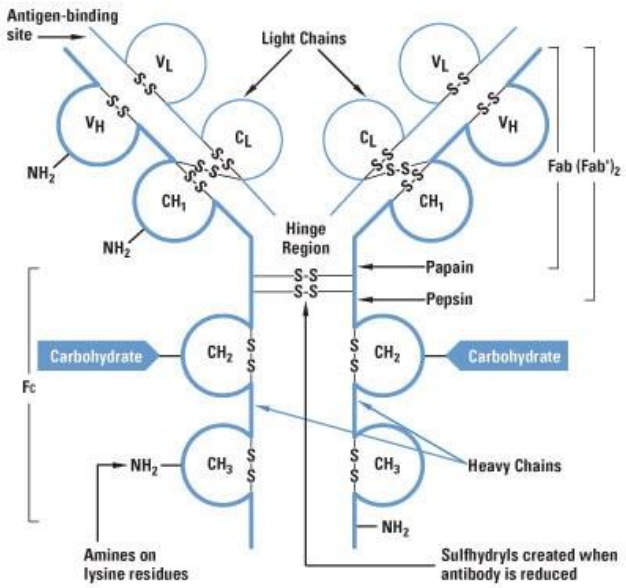

Figure 7: Antibody's functional groups. Source: https://www.thermofisher.com/es/es/home/life-science/protein-biology/protein-biology-learning-center/protein-biology-resource-library/pierce-protein-methods/overview-detection-probes.html

For instance, antibodies have several amino groups located in different parts of their structure, so a random orientation will be obtained if they are employed in the bioconjugation reaction. On the other hand, if the antibody interacts with the QD through the carbohydrates, its orientation can be controlled so that it ends-up in an end-on disposition. A third option consists in binding the antibody through the thiol groups present on the hinge region (Figure 7). This method could disrupt antibody's tertiary conformation, as the hinge region is located on its inner part. Using the enzymes papain or pepsin, the antibody can be fragmented so only the Fab or the $(Fab')_2$ regions, respectively, bind to the QD. As the paratopes are located on those regions, the antibody remains active, recognizing the antigen (*47*). Finally, affinity interactions are based on the reversible binding between two complementary molecules, achieving a high stability and specificity. This method implies the labelling of both the antibody and the QD surface with two molecules which suffer a strong affinity for each other, so it allows a total control over the orientation of the former. Most common molecule pairs employed in affinity binding are A/G proteins (*48*) and avidin/biotin (*49*), which is one of the strongest interactions in nature ($K_d = 1.3 \times 10^{-15}$ M at pH 5.0). However, this latter interaction shows some specificity problems, and for that reason some avidin alternatives have been designed, as streptavidin or NeutraLite™ avidin (*50*). Antibodies modification can be

done through amino groups, although as in the case of covalent interactions, that would lead to a random orientation. Biotinylation at the thiol groups of the hinge region has been proved as a suitable alternative, leading to an end-on orientation of the antibody.

Another concern when facing antibody-QD bioconjugation is the extent of the reaction. IgG dimensions are around 8.4 x 13.7 nm (*51*) and QD diameter is comprised in the 2-8 nm range (*52*). As a consequence of this, a variable number of QDs can be attached to each Ab, making necessary the characterization of the antibody-QD bioconjugate, so the intensity observed can be correlated with the analyte concentration. The same techniques employed for the characterization of QDs, i.e. optical measurements, ICP-MS, AF4 and DLS, can be employed for the characterization of the bioconjugates.

C. OBJECTIVES

In this work, a sandwich-like immunoassay employing QDs as luminescent probes for the detection of prostate specific antigen (PSA, a prostate cancer biomarker) will be evaluated and tested.

To achieve this objective it will be necessary to attempt these specific goals:

1. To synthesize and characterize doped QDs:
    a. Cysteine coated Mn:ZnS QD will be synthesized through a bottom-up approach. An organic procedure for the substitution of Cysteine ligands by dihydrolipoic acid (DHLA) will be developed and performed, increasing QDs stability at physiological pH. This bidentate ligand contains carboxyl groups on its structure, which can be used for the bioconjugation reaction with antibodies through the EDC/NHS reaction.
    b. The required skills for their characterization using several techniques, such as phosphorescence and ICP-MS, will be learned and tested, so their size, morphology, composition, concentration, and therefore, their emission, can be controlled.
2. Evaluation of bioconjugation efficiency. Several Ab:QDs ratios will be synthesized and their different emission spectra will be recorded, so bioconjugate emission properties can be optimized.
    a. To check bioconjugation efficiency, free and bioconjugated QDs will be separated by ultrafiltration, and phosphorescence measurements will be taken using a spectrophotometer from both the supernatant and the filtrate.
    b. To verify that Ab do not lost their recognition ability during the bioconjugation reaction, an enzymatic immunoassay employing peroxidase-labelled Ab will be performed and, after that, a sandwich plate fluorescence immunoassay will be designed and tested with the goal of detecting PSA, using both room temperature phosphorescence (RTP) and ICP-MS measurements, determining the presence of Mn and Zn.

D. MATERIALS AND METHODS

D.1. Reagents

All chemical reagents used were of analytical-reagent grade and used as received, without any further purification. Phosphates buffer solution (PBS) at pH 7.4 and sodium borate buffer (SBB) at pH 11 were already prepared in the laboratory and ready to use. Zinc chloride, manganese chloride tetrahydrate, L-Cysteine hydrochloride monohydrate and Mn and Zn 1000 ppm standards were purchased from Merck (Germany). Sodium sulfide nonahydrate, sodium bicarbonate, thioctic acid, sodium borohydride, potassium tert-butoxide, (sulfo)-N-Hydroxysuccinimide (sulfo-NHS) and 1-Ethyl-3-(3-dimethylaminopropyl)carbodiimide (EDC) were purchased from Sigma (USA). pAb anti-mouse produced in rabbit was purchased from Sigma (USA), mAb anti-PSA produced in mouse and pAb anti-PSA produced in rabbit were purchased from Abcam (UK), and horseradish peroxidase (HRP) labelled IgG anti-mouse produced in rabbit were supplied by the Scientific-Technical Services of the University of Oviedo. Peroxidase substrates, tetramethylbenzidine (TMB) and hydrogen peroxide (H_2O_2), were purchased from Thermo Fisher Scientific (U.S.A.). De-ionized Milli-Q water was employed to prepare all the solutions.

D.2. Instrumentation

Quantum Dots synthesis was performed using a JP Selecta Fibroman HT-W (Spain) heating mantle and a JP Selecta Agimatic-N (Spain) magnetic stirrer. Quantum Dots precipitation was induced using a CIC-Controltecnica Gyrozen 1580 R (Spain) centrifuge and 50 mL Falcon® Thermo Fisher (U.S.A.) tubes. Solvent evaporation was performed using an IKA RV 8 V (Germany) rotary evaporator. Phosphorescence were recorded on a Varian Cary Eclipse (Spain) luminescence spectrophotometer and absorption spectra were recorded on a Thermo Fisher Genesys 10S UV-Vis (U.S.A.) spectrophotometer, using Hellma Analytics (Germany) quartz cuvettes. Phosphorescence spectra were recorded under RTP conditions, with a decay time of 0.04 s, a delay time of 0.1 ms, a gate time of 2 ms and a detector voltage of 600 V, unless other conditions are specified. Delay time represents the time elapsed between the sample being irradiated and the emission being recorded, while gate time refers to the time that the detector spends recording data and averaging time the time that the instrument spends recording information on each

wavelength. Absorption spectra were recorded in the wavelength range 200-500 nm with 1 nm intervals. ICP measurements were performed on an Agilent 8900 ICP MS/MS (Japan) equipped with two quadrupoles (Q) and an octopole between both. QDs bioconjugation reactions were performed on 1.5 mL Labbox (Spain) Eppendorf vials placed in a TS-100C Biosan (Latvia) thermo-shaker and they were purified using a MiniSpin Eppendorf (Germany) centrifuge and 100 kDa Amicon® Merck (Germany) centrifuge cartridges. Black and clear Greiner Bio-One (Germany) ELISA plates were used as substrate for the immunoassay. Immunoassay efficiency was measured using an ELx800 Biotek (U.S.A.) absorbance microplate reader. Several HTL (Poland) micropipettes of adjustable volumes were employed. All the solutions were prepared by weight using a ME204 Mettler Toledo (U.S.A.) analytical balance and a JP Selecta Ultrasons-H (Spain) ultrasounds bath was used to facilitate the dissolution of some solutes.

D.3. Experimental section

D.3.1. *Synthesis of doped ZnS Quantum Dots*

Mn^{2+}-doped ZnS Quantum Dots were prepared following a procedure described elsewhere (*53*), with some modifications. 50 mL of L-Cysteine 0.02 M were mixed on a beaker with 5 mL of $ZnCl_2$ 0.1 M, 0.15 mL of $MnCl_2$ 0.1 M and 1.35 mL of ultrapure water, and the pH was raised to 11.8 using a saturated solution of NaOH to neutralize the hydrochloric acid present in the L-Cysteine solution, and therefore allow the deprotonation of the carboxylic and thiol groups present in the Cysteine as shown in Figure 8, which present pKa values of 1.91 and 8.14, respectively (*54*). The resultant yellowish solution was poured into a three-necked flask and it was heated and stirred for 30 minutes under Ar flux, to avoid the oxidation of the reagents or the nanoparticles once they were synthesized. The experimental setup employed during the synthesis of Mn:ZnS QDs is shown in Figure 9.

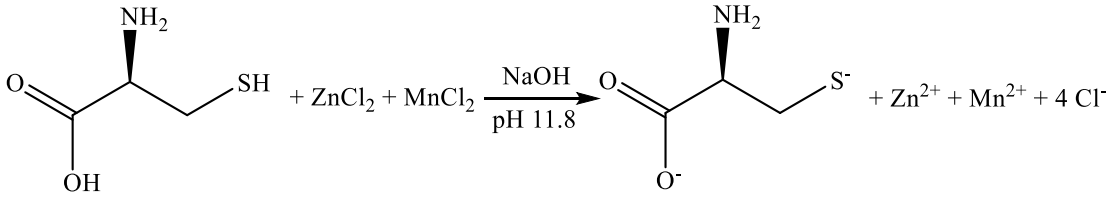

Figure 8: Species present in solution before and after alkalizing it

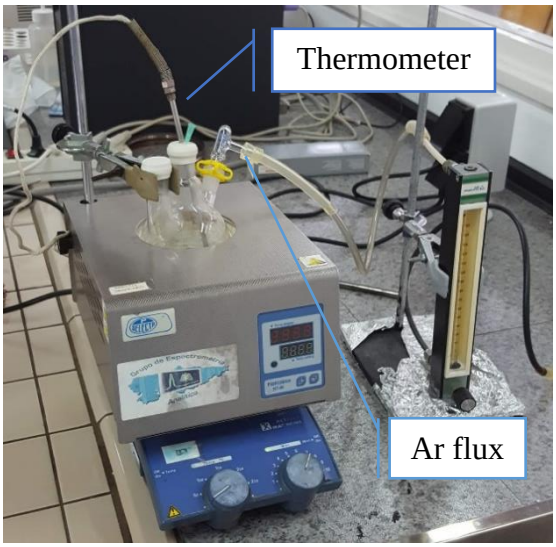

Figure 9: Experimental setup employed for the synthesis of Mn:ZnS QD

After that, 5 mL of a Na_2S 0.1 M solution were prepared and rapidly injected into the three-necked flask. The solution was left stirring for 20 more minutes, to allow QDs nucleation, according to the reaction depicted in Figure 10. Then, Ar flux was stopped and the solution was heated at 50ºC for 2 hours, to improve capping efficiency of L-Cysteine.

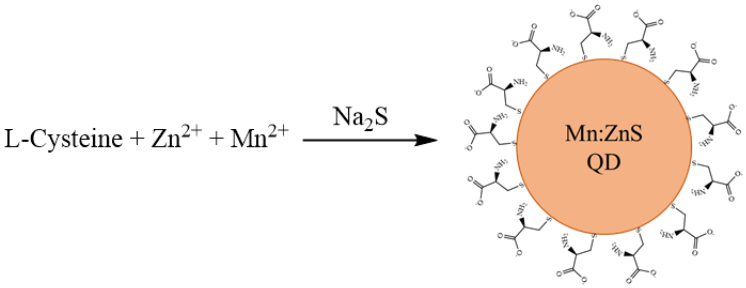

Figure 10: Synthesis of Mn:ZnS QDs capped with L-Cysteine

After the solution had rested some time at room temperature, precipitation of Mn:ZnS QDs was induced by adding an equivalent volume of ethanol to the solution and centrifuging it three times at 7500 g for 10 minutes at 4ºC. QDs synthesis methodology is summarized in Figure 11. Precipitated QDs were dried under vacuum, obtaining a dark brown powder. Cysteine capped QDs were dissolved in a sodium borate buffer (SBB) at pH 10.7 for their storage, as Cysteine is more stable at basic pH.

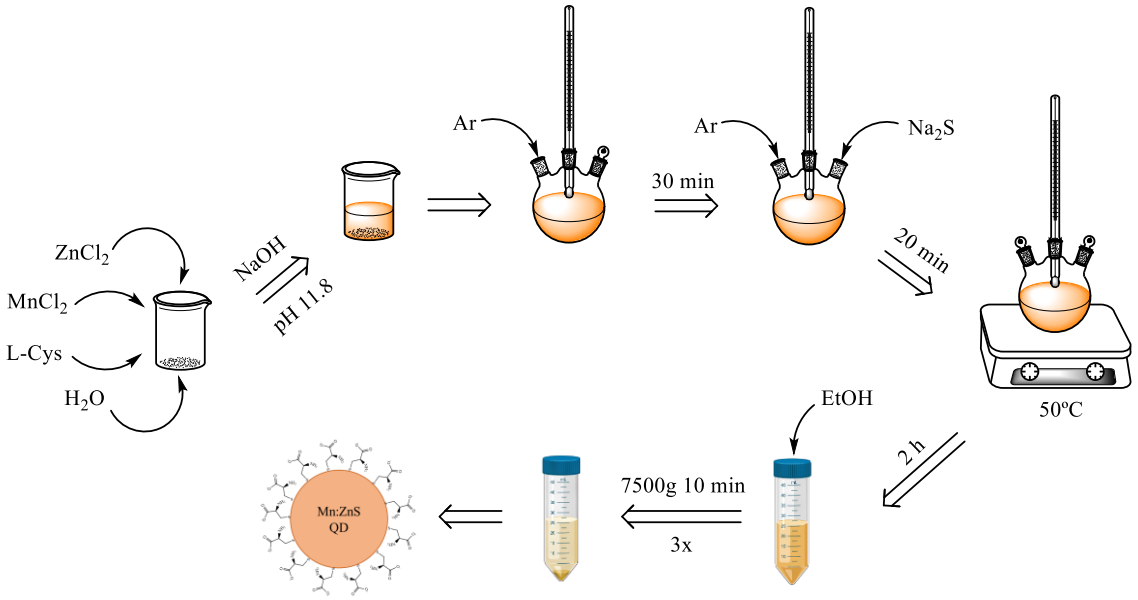

Figure 11: Quantum Dots synthesis methodology

Dihydrolipoic acid (DHLA) was prepared following a procedure described elsewhere (*55*), with some modifications. An Erlenmeyer flask was placed on an ice bath ($NaBH_4$ reaction with water is highly exothermic, producing the corresponding borate salt and hydrogen gas) and 100 mL of a 0.25 M solution of $NaHCO_3$ were added under stirring. $NaHCO_3$ main goal was to increase the pH of the solution, deprotonating the hydroxy-group present on the thioctic acid and therefore increasing its solubility in water, which otherwise would be rather low. 5 g of thioctic acid were added to the same Erlenmeyer and, after that, and very slowly due to the high volume of H_2 generated in the reaction, 1 g of $NaBH_4$, a powerful reducing agent able to break the S-S bond of the thioctic acid. Once all $NaBH_4$ was poured into the Erlenmeyer, the reaction was left under stirring over the ice bath for an hour. After that time, the solution color had changed to colorless. 100 mL of toluene were added, obtaining an organic phase with DHLA and an aqueous phase containing sodium acetate, sodium bicarbonate, the borate salt and water . The solution was acidified to pH 1 using glacial acetic acid to protonate the thiol groups and the hydroxy group present on DHLA, assuring its presence on the organic phase of the solution. Both the organic and aqueous phases were separated using a separation funnel. The organic phase was dried using magnesium sulfate and the excess of solvent was removed using a rotavapor, obtaining a viscous orange liquid (DHLA).

L-Cys capped QDs together with 800 μL of DHLA were placed in a vial and left under stirring for 2 hours. The product was redissolved in 3 mL of methanol and K[t-BuOH] was added in excess to deprotonate and precipitate QDs. The color change of the solution from yellow to green indicated that L-Cysteine was in solution. QDs were centrifuged four times at 10000 g for 10 minutes using Amicon® cartridges with a pore size of 3 kDa, and the precipitate was redissolved with ultrapure water after the first two cycles and with a phosphate buffer saline solution (PBS) 0.1 M after the third one. The precipitate was dissolved in PBS (pH 7.4) and stored in a vial. All the bioconjugation reactions were performed on PBS, as physiological pH is required.

D.3.2. *Characterization of Mn:ZnS QDs*

D.3.2.1. Spectral characterization

Luminescence spectra were taken of both L-Cys and DHLA capped Mn:ZnS QDs to study the efficiency of the nanoparticle's synthesis and of the ligand exchange, respectively. All measurements were taken at atmospheric pressure and room temperature and using quartz cuvettes. Absorption spectra were taken using a Thermo Fisher Genesys 10S UV-Vis (Spain) spectrophotometer and quartz cuvettes. Base line was stablished using a PBS solution and a wavelength range between 200 and 500 nm was fixed.

Excitation and emission QDs phosphorescence spectra were recorded using a Varian Cary Eclipse (Spain) luminescence spectrophotometer described in D.2 instrumentation section. For emission measurements, the wavelength range was fixed between 450 and 750 nm, whereas for excitation measurements it was fixed between 200 and 400 nm, unless other conditions are specified. Emission and excitation slit widths, as well as emission and excitation wavelengths, were adjusted in each measurement, as it will be discussed in the results section.

D.3.2.2. Inductively coupled plasma spectrometry (ICP-MS)

DHLA capped Mn:ZnS QDs were analyzed by ICP-MS, so QDs molar concentration in the sample could be estimated according to the equation proposed by García-Cortés *et al.* (*39*), so the Ab:QD stoichiometry could be controlled by the time of performing the bioconjugation. QDs were digested prior ICP characterization, adding 300 μL of aqua

regia to 50 µL of each QDs solution and placing the mixture on an ultrasounds bath for half an hour. Then, 200 µL of that solution were taken to 5 mL with ultrapure water.

ICP measurements were performed using an Agilent 8900 ICP MS/MS (Japan), equipped with an electron capture detector. The first quadrupole was adjusted to filter only the masses of the QDs metallic elements, i.e. 55 ($^{55}Mn^{+}$), 64 ($^{64}Zn^{+}$) and 66 ($^{66}Zn^{+}$). The abundance of the main constituent elements of air, such as C, N, O or H, the main component of the plasma (Ar) and of some trace elements present in the solvent of the solution injected (such as S coming from sulfites present in water) is huge with respect to the one of the analytes, so the formation of dimers or even trimers among these elements is frequent. Some of these aggregates can have the same mass as the analytes, like in the case of $^{40}Ar^{14}N^{1}H^{+}$ (m/z=55), $^{36}Ar^{14}N^{14}N$ (m/z=64) or $^{34}S^{16}O_2^{+}$ (m/z=66), so they will cross the first Q together with the target elements receiving the name of polyatomic interferences. To reduce the effect of these interferences, helium was introduced in the collision chamber at a flow rate of 4.5 mL/min. He is an inert gas, so it will randomly collide with all the atoms that cross the collision cell, reducing their kinetic energy. However, polyatomic interferences cross-sectional area is bigger than the one of the analytes, as they are composed by two or more atoms, so statistically He is going to collide more with them. By stablishing a kinetic energy discrimination (KED) barrier after the collision cell, only the analytes will arrive to the second Q. This filter was fixed again at the same masses than the first one, so only the target elements will arrive to the detector. This disposition of MS/MS instruments is called “on mass”, as both quadrupoles are fixed at the same m/z, and it is schematically represented in Figure 12.

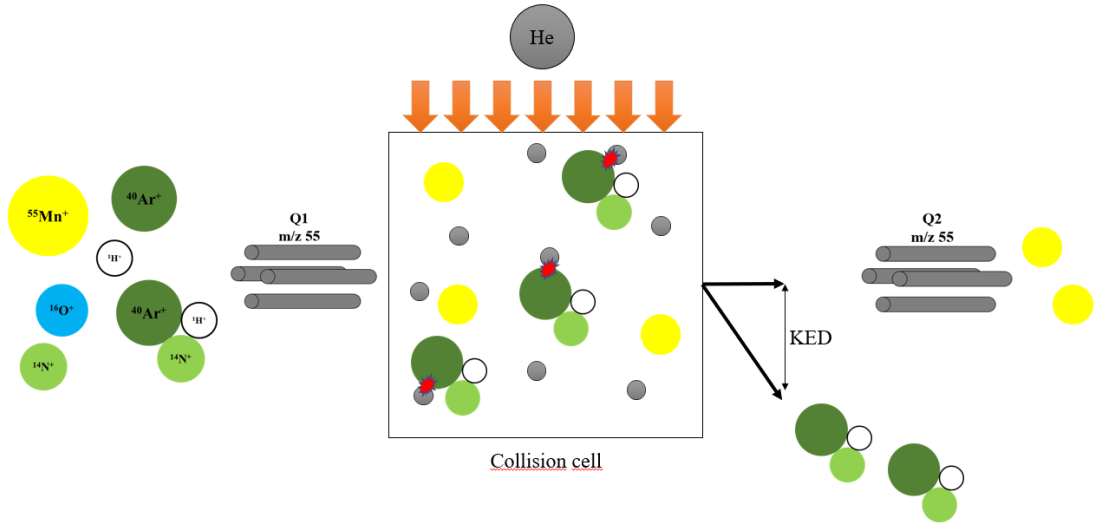

Figure 12: On mass operational mode of a MS/MS ICP-MS

$^{55}Mn^{+}$, $^{64}Zn^{+}$ and $^{66}Zn^{+}$ were measured in tenfold with an integration time of 1 s. Two Zn isotopes were measured to reduce the effect of a second type of interferences, produced when two different elements present isotopes with the same mass: isobaric interferences. For instance, $^{64}Zn^{+}$ is the mayor isotope of Zn with a 48.63% abundance, but it is interfered by $^{64}Ni^{+}$, so it is preferable to measure $^{66}Zn^{+}$, even if it is less abundant (27.90%). A previous calibration was performed employing Mn and Zn standards of increasing concentrations, from 0 to 60 ppb in the case of Mn and from 0 to 100 ppb in the case of Zn, prepared from 1000 ppm standards of each element purchased from Merck (Germany). All solutions introduced were prepared in HNO_3 2%. Acidic medium was used so all compounds were stabilized.

D.3.3. *Bioconjugation of Quantum Dots*

Bioconjugation reactions between d-dots and anti-mouse IgG produced in rabbit were performed through EDC/NHS reaction taking advantage of the carboxylic groups present in DHLA, following a procedure described elsewhere (*56*), with some modifications. In this work, different Ab:QDs ratios (1:1, 1:3, 1:5, 1:10 and 1:30) were tested, in order to optimize the efficiency of the immunoassay, with a constant Ab concentration of 1 μg/mL. Bioconjugation reactions were carried out in 1.5 mL Eppendorf tubes while shaking at constant temperature (25ºC). All the solutions were taken to a final volume of 500 μL using a PBS/0.05% Tween 20 solution (Tween 20 is a surfactant, added to avoid the adsorption of Ab to the vial walls). First, the corresponding volume of the PBS/0.05% Tween and the equivalent volume of the QDs solution to achieve the aforementioned Ab:QDs ratios were added to each Eppendorf tube. Then, (sulfo)-N-Hydroxysuccinimide (NHS) and 1-Ethyl-3-(3-dimethylaminopropyl)carbodiimide (EDC) were added in excess with respect to the QDs concentration (3000:1500:1 EDC:NHS:QD molar ratios), and the mixture was let to react for 10 minutes under shaking. This allowed the activation of the QDs surface by the EDC/NHS reaction, as depicted in Figure 13. In the first place, EDC, which is highly water soluble, reacts with the carboxylic groups present on DHLA forming an active intermediate called O-acylisourea. This intermediate could react directly with the amine groups present on Ab, but this reaction is easily reverted at an early stage. For that reason, (Sulfo)-NHS, water soluble analog of NHS, was added. As

in the case of EDC, (Sulfo)-NHS is an amine-reactive species, so when Ab were added they were able to bioconjugate to QDs forming an amide bond.

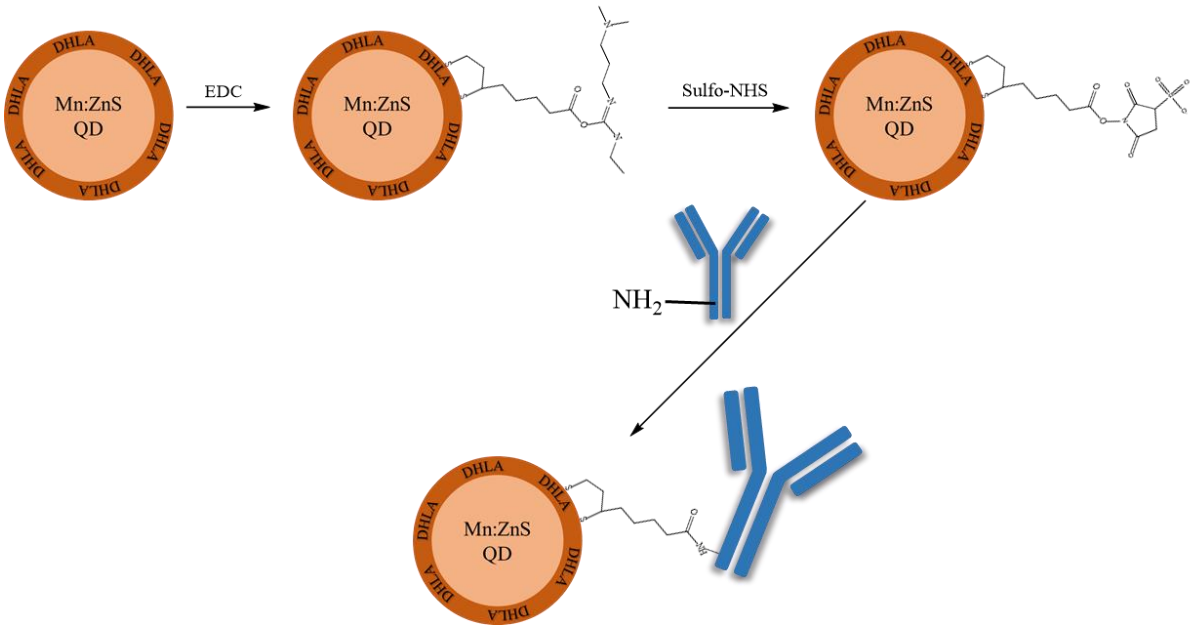

Figure 13: Quantum Dot bioconjugation reaction to antibodies through EDC/NHS reaction

Finally, a concentration of 1 μg/mL of anti-mouse IgG produced in rabbit was added to each Eppendorf and the mixture was let to react for another two hours under shaking.

After that time, each solution was transferred to a 100 kDa Amicon® and centrifuged at 13000 rpm for 10 minutes. As IgG size is usually around 150 kDa, both free IgG and QD-bioconjugated to Abs should be retained by the cartridge, while free QDs should cross it and end in the filtrate. However, in order to evaluate the efficiency of the filtration procedure, the first filtrate was stored in a vial and its phosphorescence spectra were recorded. The retained fraction was redissolved in PBS and centrifuged again twice, discarding the filtrate after each cycle. After the last cycle, the retained fractions were redissolved in PBS, stored in a vial and the emission spectra for each Ab:QD ratio was recorded.

D.3.4. *Spectrophotometric immunoassay*

A spectrophotometric immunoassay was performed to observe if anti-mouse IgG preserved its molecular recognition ability after its bioconjugation to QDs . This assay was designed according to the scheme depicted in Figure 14.

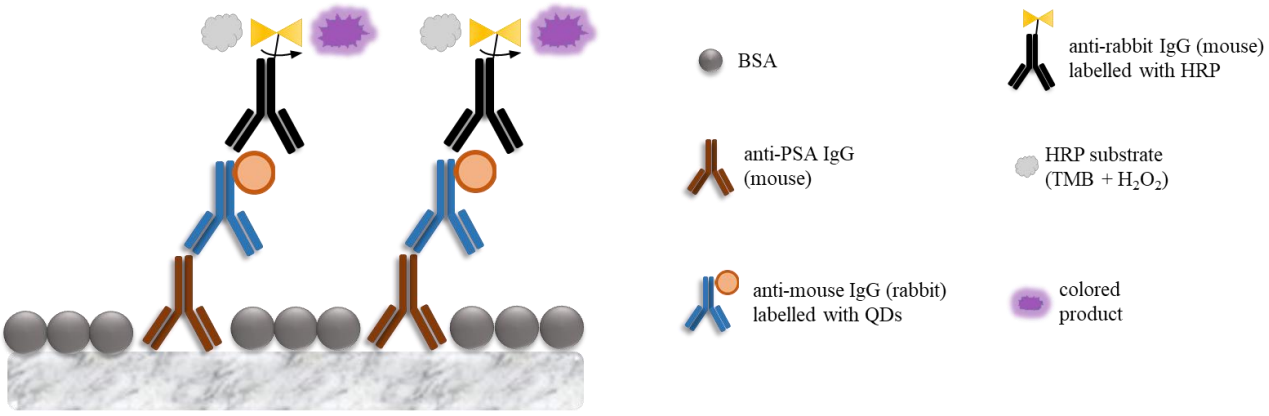

Figure 14: Spectrophotometric immunoassay

First, 100 µL of a 3 µg/mL solution of mAb anti-PSA prepared in PBS were added to wells B:G/2:4 of an ELISA plate. The plate was placed then in a stove at 35ºC for an hour, and then moved to the fridge overnight. After that, 150 µL of BSA 3% were added to each well, and the plate was placed in the stove again for other 2 hours. Then, each well was washed by triplicate using 150 µL of a PBS/Tween 20 solution and 100 µL of the different anti-mouse Ab:QDs bioconjugates, plus a free Ab sample working as blank, were added in triplicate. The plate was again placed in the stove for 2 hours, and after that time, 100 µL of an anti-rabbit Ab labelled with horseradish peroxidase (HRP) solution prepared in BSA 1% were added to each well, and the plate was left in the stove for an extra hour. After that, the plate was washed again using PBS/Tween 20, and 50 µL of 3,3',5,5'-Tetramethylbenzidine (TMB) and 50 µL of H_2O_2 were added to each well, and the plate was moved to the stove for 10 minutes. Lastly, 50 µL of H_2SO_4 2M were added to each well, and their absorption were measured using a micro-plate spectrophotometer.

D.3.5. *PSA immunoassay*

An immunoassay for the detection of PSA was designed following the scheme depicted in Figure 15. This format presents a great advantage compared to the classical sandwich immunoassay depicted in Figure 5, which is that labelled Ab is not specific towards the target analyte. For that reason, if several analytes were going to be studied, there would be no need to repeat the laborious and time-consuming bioconjugation process, but only to change the primary antibody.

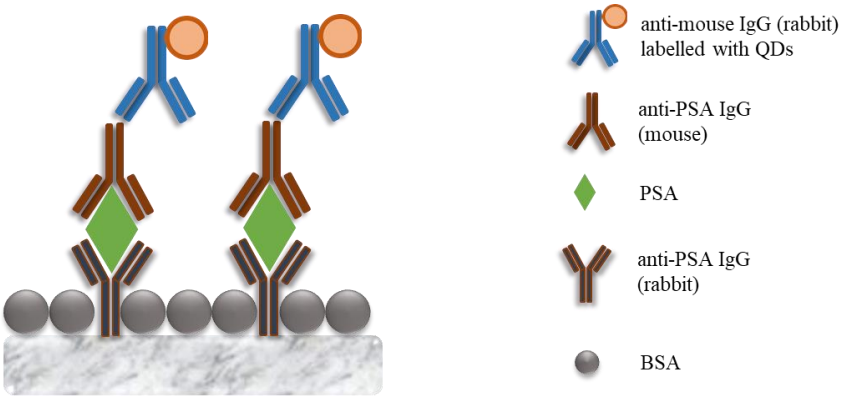

Figure 15: Immunoassay for the detection of PSA

4 mL of an Ab:QD solution, in a 1:30 proportion, were prepared following a similar procedure as the one described formerly in this work (D.3.3 section), and bioconjugation efficiency was checked by phosphorescence measurements. 100 µL of a 5 µg/mL solution of pAb anti-PSA produced in rabbit prepared in PBS were added to wells B:G/2:4 and B:G/7:9 of a black ELISA plate, and the plate was let to upholster in the stove for an hour. The plate was blocked using BSA 3% for two hours in the stove, and 10 standards of increasing PSA concentrations from 0 – 500 ng PSA/mL were prepared in PBS (each standard was prepared in triplicate). The blank solution was prepared using BSA 1%. After 2 hours in the stove and the corresponding PBS/Tween 20 washes, 100 µL of 3 µg/mL solution of mAb anti-PSA produced in mouse were added to each well, and after other 2 hours in the stove, 100 µL of the Ab:QDs solution were added.

D.3.5.1. Phosphorescence measurements

Phosphorescence emission spectra of the different wells were recorded using a Varian Cary Eclipse (Spain) luminescence spectrophotometer equipped with a plate reader and the operating conditions already described in D.2 instrumentation section, with a fixed excitation wavelength of 314 nm and an emission wavelength of 590 nm. Plate height was adjusted before the measurements.

D.3.5.2. ICP-MS measurements

All the wells were digested using aqua regia and an ultrasounds bath. Their content was transferred to a 2 mL Eppendorf vial and each solution was taken to a final volume of 1.5 mL with ultrapure water.

ICP measurements were performed using an Agilent 8900 ICPQQQ (Japan) (see D.2 instrumentation section), using the same conditions as the ones employed for QDs characterization (D.3.2.2 section). A previous calibration was performed employing Mn and Zn standards of increasing concentrations, from 0 to 20 ppb in the case of Mn and from 0 to 300 ppb in the case of Zn, prepared from 1000 ppm standards of each element purchased from Merck (Germany).

E. RESULTS AND DISCUSSION

E.1. QDs optical characterization

Absorption spectrum for DHLA capped QDs was taken using a diluted QDs solution to avoid the saturation of the signal. As it can be observed in Figure 16, a maximum absorption was observed at 281 nm, which was used as a reference value for phosphorescence emission measurements.

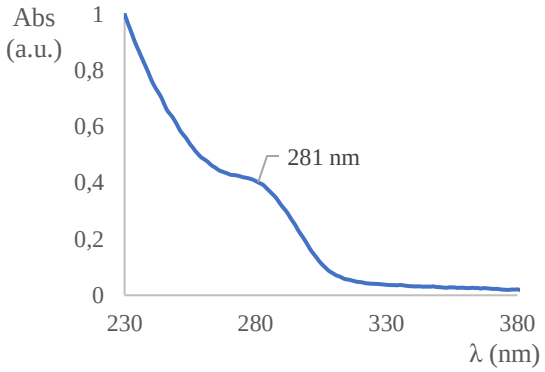

Figure 16: Absorption spectrum for DHLA capped Quantum Dots

Phosphorescence emission spectra for both L-Cys capped and DHLA capped Mn:ZnS QDs were recorded initially with excitation and emission slits of 10 nm.

Emission spectrum for L-Cys capped QDs was measured at an excitation wavelength of 285 nm, showing a well-defined emission peak at 593 nm, which is in accordance with the bibliography (*56*). To know exactly at which wavelength occurred the excitation, an excitation spectrum was then recorded, at the emission wavelength obtained (593 nm). The maximum obtained (306 nm) was used to measure again the emission spectrum, this time obtaining a peak at 591 nm, more intense than the first one (Figure 17).

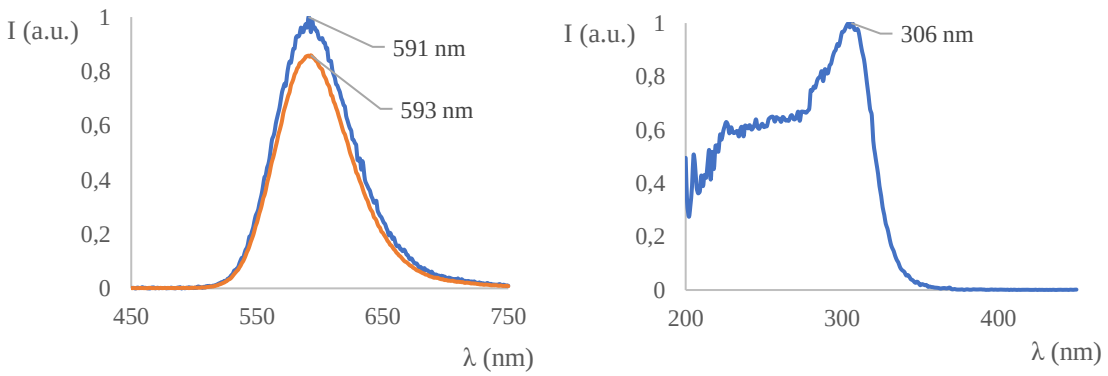

Figure 17: Different spectra for L-Cys capped QDs. Left: emission spectrum recorded at λ_{ex}=285 nm (orange) and at λ_{ex}=306 nm (blue); right: excitation spectrum recorded at λ_{em}=593 nm

After that, to characterize DHLA capped QDs, emission spectrum was recorded measuring at the excitation wavelength of 306 nm and a low intensity peak, with a low signal to noise ratio was observed. This could be due to several factors: low recoveries during QDs separation, low QDs concentration in the sample, human errors at any step of the process, etc. A second spectrum of the same sample was performed, increasing the slit widths to 20 nm, but the spectrum did not improve significantly. To augment QDs signal, a second ligand exchange was performed on another L-Cys capped QDs fraction, increasing both centrifuge time and speed, trying to maximize the recoveries after each step. This second fraction showed remarkable phosphorescence intensity, even with slit widths of 5 nm (Figure 18). An excitation spectrum of this second sample was also recorded, obtaining again a λ_{ex}=306 nm. These results confirmed that DHLA capped QDs were synthesized satisfactorily according to their optical properties.

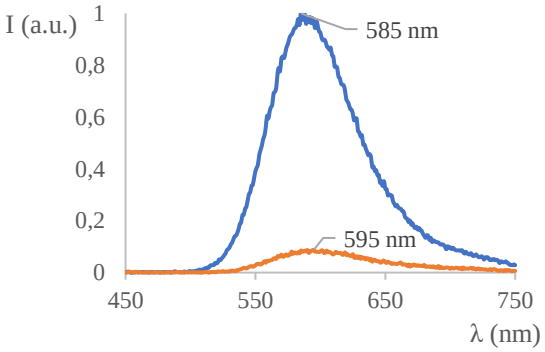

Figure 18: Emission spectrum for DHLA capped QDs after the first ligand exchange with 20 nm slits (orange) and after the second ligand exchange with 5 nm slits (blue)

E.2. QDs ICP characterization

After confirming QDs optical properties, the following step was to characterize synthesized QDs by ICP-MS. Firstly, a calibration of individual metal parts of QDs was performed. Calibration signals were adjusted to a linear model for each element measured (Figure 19). A weighted regression line was calculated also for each element, obtaining the following signal-concentration relationships:

Cps ^{55}Mn = 4590053.345 [^{55}Mn] (ppm) + 115.353 (R^2 = 0.995)

Cps ^{64}Zn = 1503614.964 [^{64}Zn] (ppm) + 3070.557 (R^2 = 0.997)

Cps ^{66}Zn = 959305.248 [^{66}Zn] (ppm) + 1893.787 (R^2 = 0.998)

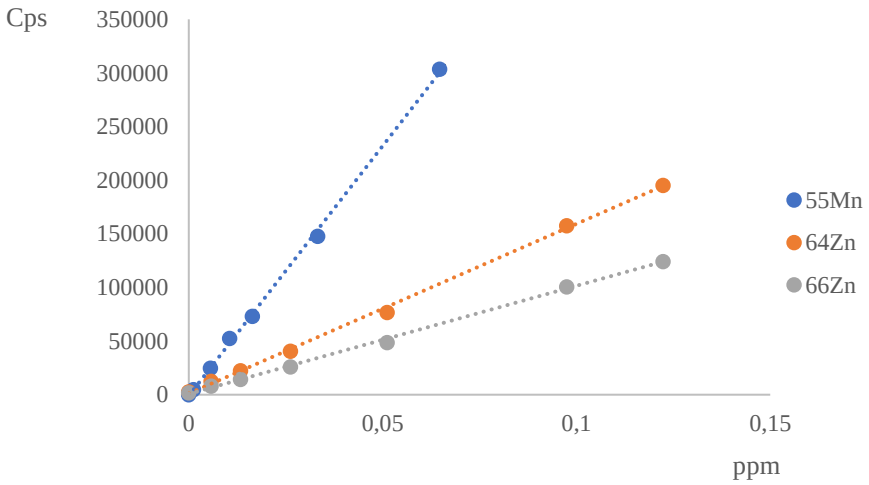

Figure 19: Linear regression for each element measured in the calibration for Quantum Dots characterization

Mn and Zn concentrations in the synthesized QDs were obtained using the weighted regression line equations, obtaining values of 2.86 ± 0.51 ppm of Mn and 62.1 ± 4.5 ppm of Zn, which correspond to 7.0 ± 1.3 µg of Mn and 152 ± 11 µg of Zn, respectively. The molar ratio Mn/Zn present in the QDs was 5.49 %, higher than the 3 % expected according to the amounts of each reagent employed in the synthesis. Possible explanations for these results could be related to errors during the synthesis, such as a higher $MnCl_2$ concentration than needed, or higher Mn^{2+} ions intrusion in the ZnS lattice than expected.

After obtaining Mn/Zn molar ratio, QDs concentration was calculated. According to García-Cortés *et al.* (*39*), QDs concentration can be obtained through Equation 1, where M_{Zn} represents the total mass of Zn present on the sample, measured by ICP-MS; x_{blende} represents the fraction of the QD mass which is in the crystalline phase as blend (the rest of it corresponds to an amorphous phase); n_{Zn}^{at} represents the number of Zn atoms per QD and A_w^{Zn} represents the atomic weight of zinc (65.38 u).

$$c_{QDs}(\mu mol) = \frac{M_{Zn}(\mu g) \times x_{blende}}{n_{Zn}^{at} \times A_w^{Zn}} \qquad \text{(Equation 1)}$$

x_{blende} and n_{Zn}^{at} can be easily obtained through XRD measurements. x_{blende} strongly depends on % Mn on the sample (*36*), although in this work a value of 0.97 was assumed as the molar fraction of blende, in agreement with the published bibliography (*39*), as it was not

possible to perform XRD measurements. Similarly, a value of 155 zinc atoms per QD was assumed (*39*). From the zinc mass of the sample calculated from the ICP-MS results, a value of 0.0145 ± 0.0010 μmoles of QDs on the sample was estimated, which correspond to a concentration of 5.94 ± 0.43 μM (RSD = 7.18 %).

E.3. Ab:QD ratio optimization

Once synthesized QDs were characterized, a bioconjugation efficiency evaluation was performed, separating by ultrafiltration free and bioconjugated QDs and characterizing by phosphorescence measurements both the retained and the filtrate fractions, for each Ab:QDs ratio. It can be observed in Figure 20 how the intensity of both fractions increases as the QDs proportion with respect to the Ab increases, although this variation is significantly higher in the case of the retained fraction. From the emission spectrum of the retained fraction, it can be easily concluded that the Ab:QD ratio that provides the higher emission intensity was 1:30, so this was the fraction chosen to perform the immunoassay.

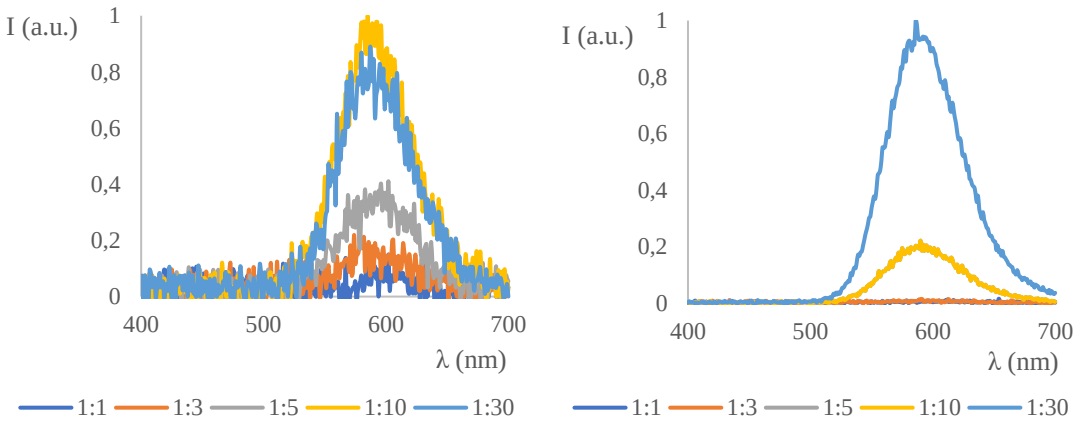

Figure 20: Phosphorescence intensity of the filtrate (left) and retained (right) fractions of the different Ab: QDs ratios

In addition, it can be observed in Figure 21 how the emission intensity of the retained fraction is much higher than the one of the filtrates. During the purification, 100 kDa Amicon® filters were used, so only free QDs could go through them. The retained fraction emission being far more intense than the filtrate fraction emission indicates that

the efficiency of the bioconjugation reaction was high, as only a small amount of QDs remained unbound.

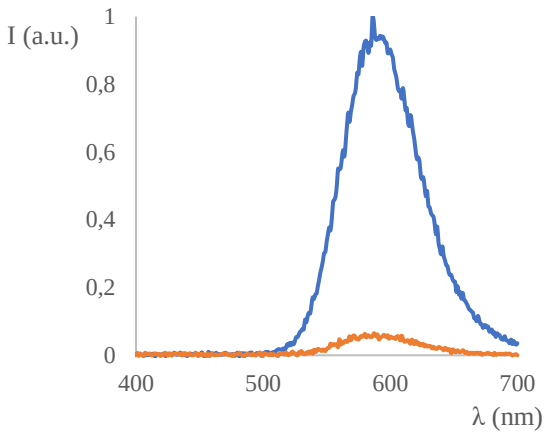

Figure 21: Emission intensity of the 1:30 retained fraction (blue) and of the filtrate fraction (orange)

E.4. Spectrophotometric immunoassay

The next step was to verify that Abs did not lose their recognition ability during the bioconjugation reaction. To attempt this study, an enzymatic immunoassay employing peroxidase-labelled Ab was performed, according to the scheme showed in Figure 22.

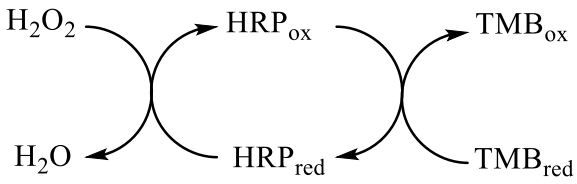

Figure 22: Enzymatic reaction catalyzed by HRP

HRP catalyzes the oxidation of TMB producing a blue-colored product (TMB_{ox}). By adding H_2SO_4, the pH is reduced below the working range of HRP, so the enzyme becomes inactive. As a direct consequence, TMB oxidation is stopped, so the intensity of each well can be directly correlated with the amount of enzyme (i.e. the amount of QD labelled anti-mouse IgG) present on each sample, being independent of the moment when it was measured. Medium acidification has another consequence, the conversion of

TMB_{ox} to a diimine yellow product, with a maximum absorbance at 450 nm. The results obtained, which can be observed in Figure 23, shows an increasing absorbance intensity as the Ab:QDs ratio increases, with a maximum signal corresponding to free anti-mouse IgG (it was the only sample not purified).

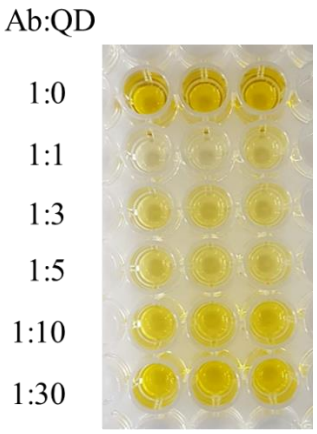

Figure 23: Spectrophotometric immunoassay results for different Ab:QD ratios

A possible explanation for these results can be found in the purification step. As the Ab:QDs ratio increases, the probabilities of a certain antibody not getting attached any QDs to its surface diminishes, so most Ab would be retained by the Amicon® filter. On the other hand, at low Ab:QDs ratios, it would be more likely that several Ab would end up with no QDs attached, so they would either cross the filter or get stick to it. Another possibility was that QDs were able of catalyze by themselves the oxidation of TMB, so at higher QDs concentration, more color would be observed, even though less HRP was present. To test this option, TMB and H_2O_2 were added to a QDs solution, without HRP-labelled IgG, to check if some color was observed. However, after the addition of H_2SO_4, the solution remained colorless, so this possibility was discharged. Nevertheless, the spectrophotometric assay proved that anti-mouse IgG recognition ability towards anti-PSA IgG was not affected by the bioconjugation reaction.

E.5. PSA-specific immunoassay

The final testing of the evaluated and optimized sandwich plate immunoassay was the quantification of PSA, using both room temperature phosphorescence (RTP) and ICP-MS measurements, determining the presence of Mn and Zn.

E.5.1. *Phosphorescence measurements*

PSA analysis was carried out by plate phosphorescence emission was measured under a delay time of 0.1 ms, a gate time of 2 ms, an excitation wavelength of 314 nm, an averaging time of 0.01 s, emission and excitation slits of 20 nm, a detector voltage of 900 V, a wavelength range from 450 nm to 750 nm and a Savitzky-Golay smoothing with a window of 15 points.

Results have shown, although slight, a relationship between emission intensity and PSA concentration, as it is shown in Figure 24. After some data treatment, the results fitted to a logarithmic regression (I (a.u.) = 0.0492ln[PSA] (ng/mL) + 3.6536, R^2 = 0.904), using the data for a wavelength of 592 nm (Figure 24). However, sensibility was quite low, so a second immunoassay was designed. A possible explanation for this low sensibility could reside in the color of the ELISA well-plate used (black), which could absorb part of the emitted radiation. In the second assay, a clear plate with a white sheet of paper attached beneath was used, simulating a white plate (which was not available in the laboratory by the moment of performing the immunoassay).

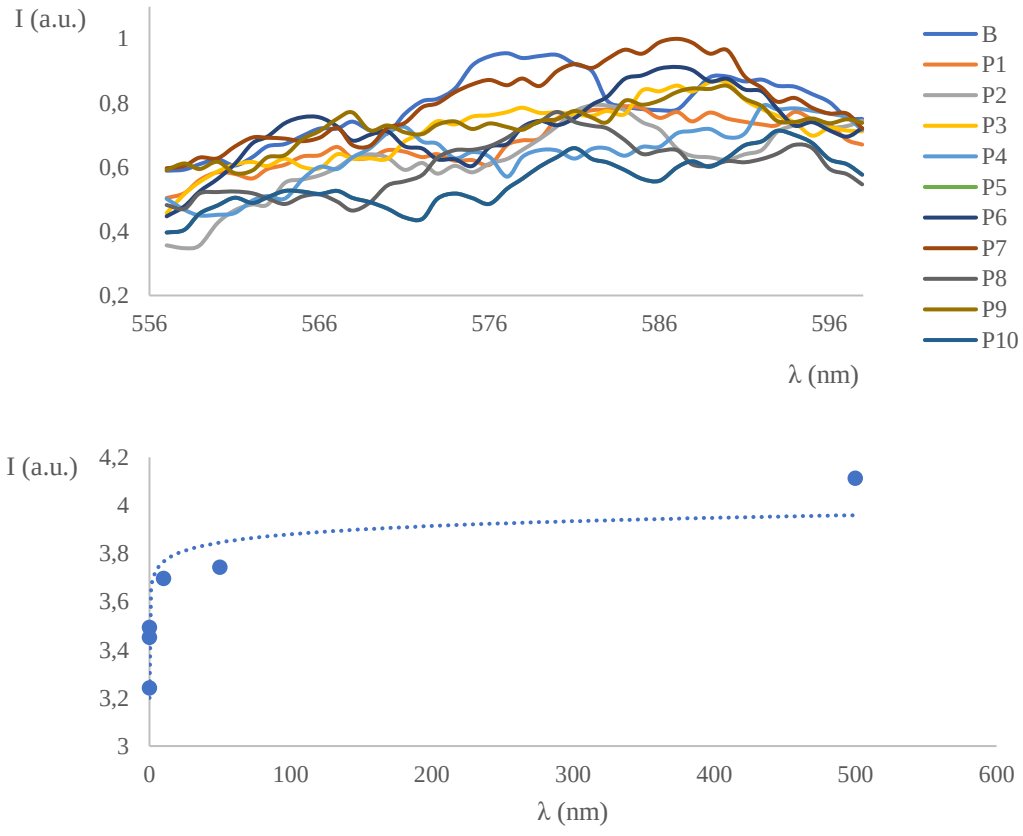

Figure 24: Plate phosphorescence emission intensity of the different standards (up) and calibration plot for the intensities at 592 nm (down)

The conditions for the second immunoassay, performed on a clear plate, were a delay time of 0.1 ms, a gate time of 5 ms, an excitation wavelength of 306 nm, an averaging time of 0.01 s, emission slit of 20 nm and excitation slit of 10 nm, a detector voltage of 900 V, a wavelength range from 450 nm to 700 nm and a Savitzky-Golay smoothing with a window of 15 points. This second immunoassay was performed in triplicate, and averaging the data the spectrum showed in Figure 25 was obtained.

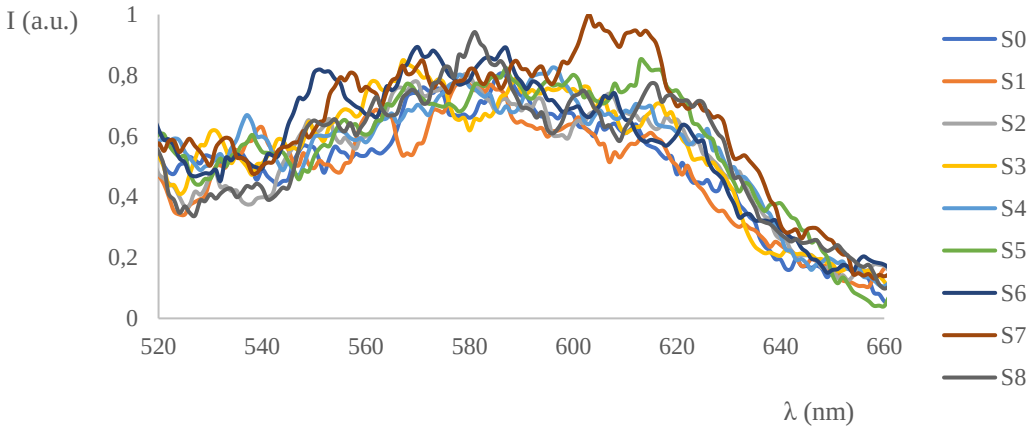

Figure 25: Plate phosphorescence emission intensity of the different standards for the second immunoassay

Although no conclusive data could be obtained from this spectrum, in which a significant increase in the signal with PSA concentration cannot be observed, when emission intensities at 587 nm were plotted versus PSA concentrations, a great fit to a logarithmic curve was obtained (I (a.u.) = 0.4406ln[PSA] (ng/mL) + 27.7506, R^2 = 0.934), as it can be observed in Figure 26. In addition, compared with the previous calibration, greater sensibilities were obtained, with higher intensity variations with respect to PSA values.

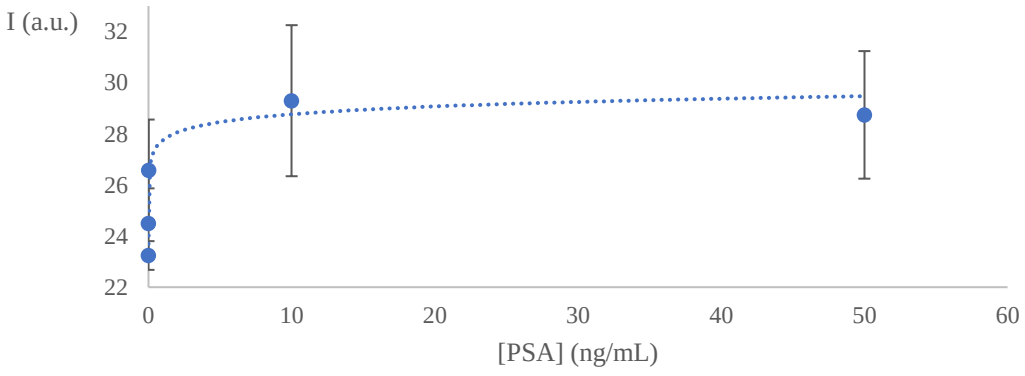

Figure 26: Calibration plot for the intensities at 587 nm for the second immunoassay

A limit of detection (LOD) of 2.54 ng PSA/mL was obtained, calculated from the intensity of the blank signal plus three times its standard deviation, which is an acceptable value taking into account all the factors that affect plate phosphorescence measurements, both internal (such as the low volume present on each well, 100 µL, or the low QDs concentration) and external (such as an optical malfunction or an inaccurate plate disposition in the spectrophotometer).

A.1.1. *ICP-MS measurements*

A real sample was prepared adding PSA up to a final concentration of 1 ng/mL to a solution of synthetic urine, prepared following a procedure described elsewhere (*57*). This matrix was chosen as it represents a realistic approach, since PSA is usually measured either in serum or in urine samples.

First, a weighted calibration for ^{55}Mn, ^{64}Zn and ^{66}Zn was performed and adjusted to a linear model through the following equations, all of them presenting excellent coefficients of determination, and as depicted in Figure 27:

Cps ^{55}Mn = 14267.183 [^{55}Mn] (ppb) + 2493.305 (R^2 = 0.999)

Cps ^{64}Zn = 5475.495 [^{64}Zn] (ppb) + 18420.372 (R^2 = 0.999)

Cps ^{66}Zn = 3471.009 [^{66}Zn] (ppb) + 11657.632 (R^2 = 0.999)

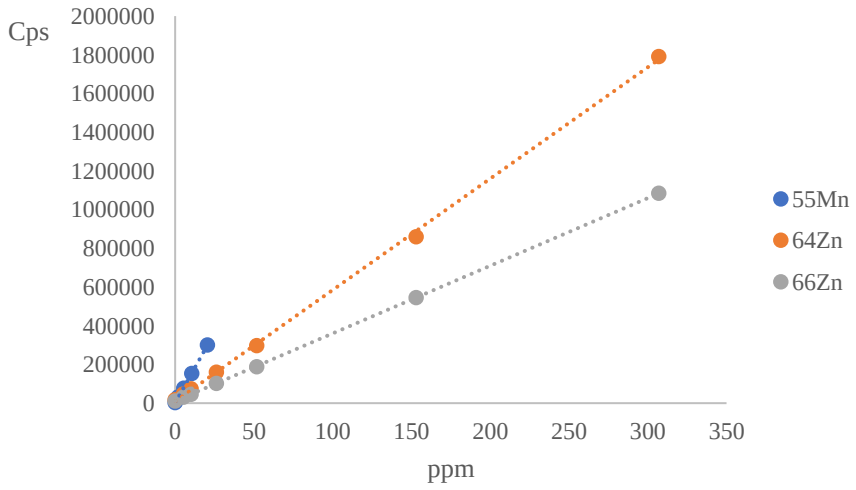

Figure 27: Linear regression for each element measured in the calibration for PSA quantification

After that, PSA standards were injected and measured by the ICP. The obtained Cps_{Metal} vs [PSA] was converted to [Metal] vs [PSA] using the calibration equations obtained for each element. By doing that, the exact concentration of each solution was considered, instead of assuming a round number, so more accurate results were obtained. The results obtained both for ^{66}Zn and ^{55}Mn are depicted in Figure 28, showing good fits to a logarithmic regression for both Zn ([^{66}Zn] (ppb) = 24.536ln[PSA] (ng/mL) + 604.686, R^2 = 0.939) and Mn ([^{55}Mn] (ppb) = 3.0071ln[PSA] (ng/mL) + 67.229, R^2 = 0.969).

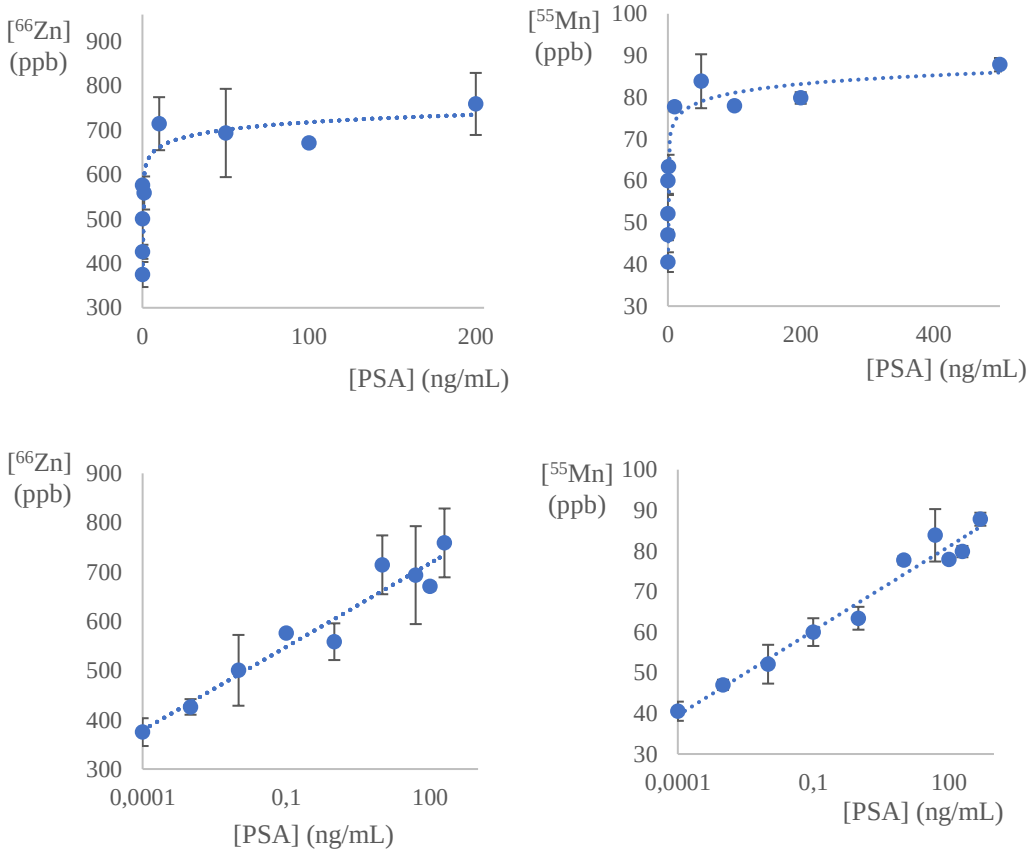

Figure 28: Calibration plot in linear (up) and logarithmic (down) scales as a function of ^{66}Zn (left) and ^{55}Mn (right) for PSA

In spite of this, the intensity value for the real sample was overestimated in both cases (800 ± 41 ppb expressed as ^{66}Zn concentration and 94 ± 1 ppb expressed as ^{55}Mn concentration), falling on the plateau of the calibration (i.e. outside its linear range), making its quantification impossible. PSA concentration added to the sample was just 1 ng/mL, so much lower intensities were expected in both cases. The explanation behind this PSA overestimation could be the complex matrix employed, which could cause some

unspecific interactions with the antibodies, so at the end QDs signal recorded cannot be correlated with PSA concentration. Nevertheless, further studies would be needed to exactly determine the nature of this situation.

On the other hand, excellent LODs were obtained for both elements, with values of 244 pg PSA/mL in the case of ^{66}Zn and 5 pg/mL in the case of ^{55}Mn.

F. CONCLUSIONS/CONCLUSIONES

In this work, a sandwich-like immunoassay for the detection of prostate specific antigen (PSA) was tested, employing manganese-doped zinc sulfide Quantum Dots (Mn:ZnS QDs) as tags. During the process, the necessary skills and knowledge required to experimentally design and perform this assay, in topics such as nanoparticles synthesis and their characterization, nanoparticles bioconjugation to biomolecules, how to perform an ELISA or how to obtain and analyze ICP-MS and luminescent data, among others, were acquired, complementing the theoretical background learned during previous courses. Regarding the results obtained, several aspects can be outlined:

-By doping ZnS QDs with Mn^{2+} impurities, a phosphorescence-like emission is obtained, with a peak around 595 nm. QDs surface modification with dihydrolipoic acid (DHLA) enhances nanoparticles stability, without altering their luminescent features.

-ICP-MS characterization allows the quantitative determination of QDs mass and composition. In addition, this information combined with additional data obtained from XRD and TEM measurements, permits the estimation of QDs molar concentration on a certain sample, a useful information when a further bioconjugation step is intended.

-When QDs are bioconjugated to antibodies, a trade-off is stablished, between trying to maximize the signal obtained without altering antibodies recognition ability. Experimentally, a 1:30 (Ab:QDs) ratio was chosen, as it successfully fulfilled both parameters, as it could be concluded from the phosphorescence measurements and the spectrophotometric immunoassay, respectively. Furthermore, QDs emission properties are not altered, so they still show a maximum emission at 595 nm.

-PSA-specific sandwich immunoassay showed great limits of detection by using both phosphorescence and ICP-MS techniques, with values of 2.54 ng PSA/mL and 244 pg PSA/mL, respectively, although PSA concentration on the real sample could not be estimated. As expected, the use of a high-performance instrument (ICP-MS 8900) provided the best results. However, due to the lack of time available as a consequence of the current sanitary situation, the recommended, if not necessary, optimizations of both assays came undone, which in both cases could lead to better results.

En este trabajo, se examinó un inmunoensayo tipo sándwich para la detección del antígeno específico prostático (PSA), empleando Quantum Dots de sulfuro de zinc dopados con manganeso (Mn:ZnS QDs) como etiquetas. Durante el proceso, las habilidades y conocimientos necesarios para diseñar y llevar a cabo este ensayo experimentalmente, en campos como la síntesis de nanopartículas y su caracterización, la bioconjugación de nanopartículas a biomoléculas, como llevar a cabo un ELISA o como obtener y tratar datos de medidas luminiscentes o por ICP-MS, entre otros, fueron adquiridos, complementando la formación teórica obtenida durante cursos anteriores. En cuanto a los resultados obtenidos, varios aspectos pueden ser destacados:

-Al dopar los ZnS QDs con impurezas de Mn^{2+}, se obtiene una emisión con características fosforescentes, con un máximo alrededor de 595 nm. La modificación superficial de los QDs con ácido dihidrolipoico (DHLA) aumenta la estabilidad de las nanopartículas, sin alterar sus propiedades luminiscentes.

-La caracterización por ICP-MS permite la determinación de la masa y composición de los QDs. Además, esta información combinada con datos adicionales obtenidos por medidas de XRD y TEM, permiten la estimación de la concentración molar de QDs en una determinada muestra, una información útil cuando se prevé llevar a cabo un bioconjugación posterior.

-La bioconjugación de los anticuerpos con los QDs exige el establecimiento de una situación de compromiso que aúne la maximización de la señal obtenida y minimice la alteración de la capacidad de reconocimiento de los anticuerpos. Experimentalmente, una proporción 1:30 (Ab:QDs) fue escogida, pues cumplía satisfactoriamente ambos parámetros, como se pudo concluir a partir de las medidas de fosforescencia y del inmunoensayo espectrofotométrico, respectivamente. Además, las propiedades luminiscentes de los QDs no se vieron alteradas, manteniendo un máximo de emisión a 595 nm.

-El inmunoensayo tipo sándwich para la detección de PSA permitió obtener buenos límites de detección tanto por medidas de fosforescencia como de ICP-MS, con valores de 2.54 ng PSA/mL y 244 pg PSA/mL, respectivamente, aunque la concentración de PSA en la muestra real no pudiera ser estimada. Como era de esperar, el uso de un equipo de alta eficacia (ICP-MS 8900) proporcionó los mejores resultados. Sin embargo, debido a la falta de tiempo por culpa de la situación sanitaria actual, las recomendadas, si no

necesarias, optimizaciones de ambos ensayos no se pudieron abordar en la extensión deseada, lo cual podría haber proporcionado mejores resultados.

G. REFERENCES

(*1*) FDA-NIH Biomarker Working Group. BEST (Biomarkers, EndpointS, and other Tools) Resource [Internet]. Silver Spring (MD): Food and Drug Administration (US); 2016-. Glossary. 2016 Jan 28 [Updated 2020 Mar 3]. Available from: https://www.ncbi.nlm.nih.gov/books/NBK338448/ (accessed Apr 28, 2020) Co-published by National Institutes of Health (US), Bethesda (MD)

(*2*) Screening tests for prostate cancer. American Cancer Society. https://www.cancer.org/cancer/prostate-cancer/detection-diagnosis-staging/tests.html#written_by (accessed June 26, 2020)

(*3*) Mashkoor, F. C.; Al-Asadi, J. N.; Al-Naama, L. M. Levels of prostate-specific antigen (PSA) in women with breast cancer. *Cancer Epidemiol.*, **2013**, *37*, 613-618

(*4*) Cevik, E. High sensitive detection of prostate specific antigen by using ferrocene cored asymmetric PAMAM dendrimer interface screen printed electrodes. *Electroanalysis*, **2019**, *31*

(*5*) Biswas, T.; Datta, A.; Sen, P. Prostate-specific antigen in females: a new tool? *J. Res. Med. Sci.*, **2011**, *16* (9), 1257

(*6*) Domon, B.; Aebersold, R. Mass spectrometry and protein analysis. *Science*, **2006**, *312*, 212-217

(*7*) Linscheid, M. W. Molecules and elements for quantitative bioanalysis: the allure of using electrospray, MALDI, and ICP mass spectrometry side-by-side. *Mass. Spec. Rev.*, **2019**, *38*, 169-186

(*8*) Lecrenier, M. C.; Marbaix, H.; Dieu, M.; Veys, P.; Sagerman, C.; Raes, M.; Baeten, V. Identification of specific bovine blood biomarkers with a non-targeted approach using HPLC ESI tandem mass spectrometry. *Food Chem.*, **2016**, *213*, 417-424

(*9*) Ryan, D. J.; Spraggins, J. M.; Caprioli, R. M. Protein identification strategies in MALDI imaging mass spectrometry: a brief review. *Curr. Opin. Chem. Biol.*, **2019**, *48*, 64-72

(*10*) Wang, M.; Feng, W. Y.; Zhao, Y. L.; Chai, Z. F. ICP-MS-based strategies for protein quantification. *Mass Spectrom. Rev.*, **2010**, *29*, 326-348

(*11*) Calderón-Celi, F.; Encinar, J. R.; Medel, A. S. Standardization approaches in absolute quantitative proteomics with mass spectrometry. *Mass Spec. Rev.*, **2018**, *37*(6), 715-737

(*12*) Medel, A. S.; Bayón, M. M.; Bettmer, J.; Sánchez, M. L. F.; Encinar, J. R. ICP-MS for absolute quantification of proteins for heteroatom-tagged, targeted proteomics. *Trends Anal. Chem.*, **2012**, *40*, 52-63

(*13*) Ong, S. E. The expanding field of SILAC. *Anal. Bioanal. Chem.*, **2012**, *404*, 967-976

(*14*) Zhang, X.; Huang, B.; Zhou, X.; Chen, C. Quantitative proteomic analysis of S-nitrosated proteins in diabetic mouse liver with ICAT switch method. *Protein Cell*, **2010**, *1* (7), 675-687

(*15*) Hajkova, D.; Rao, K. C. S.; Miyagi, M. Recent technological developments in proteolytic ^{18}O labelling. *Curr. Proteomics*, **2011**, *8*, 39-46

(*16*) Kettenbach, A. N.; Rush, J.; Gerber, S. A. Absolute quantification of protein and post-translational modification abundance with stable isotope-labeled synthetic peptides. *Nat. Protoc.*, **2011**, *6* (2), 175-186

(*17*) Ahsan, N.; Rao, R. S. P.; Gruppuso, P. A.; Ramratnam, B.; Salomon, A. R. Targeted proteomics: current status and future perspectives for quantification of food allergens. *J. Proteom.*, **2016**, *143*, 15-23

(*18*) Hermann, G.; Møller, L. H.; Gammelgaard, B.; Hohlweg, J.; Mattanovich, D.; Hann, S.; Koellensperger, G. *In vivo* synthesized ^{34}S enriched amino acid standards for species specific isotope dilution of proteins. *J. Anal. At. Spectrom.*, **2016**, *31*, 1830-1835

(*19*) Celis, F. C.; Barrio, L. C.; Encinar, J. R.; Medel, A. S.; Calvete, J. J. Absolute venomics: absolute quantification of intact venom proteins through elemental mass spectrometry. *J. Proteom.*, **2017**, *164*, 33-42

(*20*) Aitken, A.; Learmonth, M. P. Protein determination by UV absorption. In *The protein protocols handbook*, 3rd edition; Walker, J. M., Eds.; Humana Press: Totowa, New Jersey, 2009; pp 3-4

(*21*) Eck, M. Performance enhancement of hybrid nanocrystal-polymer bulk heterojunction solar cells: aspects of device efficiency, reproducibility, and stability. Ph.D. Dissertation, University of Freiburg, Baden-Württemberg, Germany, 2014

(*22*) Yalow, R. S.; Berson, S. A. Assay of plasma insulin in human subjects by immunological methods. *Nature*, **1959**, *184* (4699), 1648-1649

(*23*) Kudo, T.; Kido, A.; Nishiyama, Y.; Koganeya, H.; Okuda, T.; Nabeshima, M.; Iinuma, Y.; Ichiyama, S. Whole-blood counting immunoassay as a short-turnaround test for detection of Hepatitis B surface antigen, anti-Hepatitis C virus antibodies, and anti-*Treponema pallidum* antibodies. *J. Clin. Microbiol.*, **2004**, *42* (9), 4250-4252

(*24*) Gan, S. D.; Patel, K. R. Enzyme immunoassay and enzyme-linked immunosorbent assay. *J. Invest. Dermatol.*, **2013**, *133* (9), e12

(*25*) Boverhof, D. R.; Bramante, C. M.; Butala, J. H.; Clancy, S. F.; Lafranconi, M.; West, J.; Gordon, S. C. Comparative assessments of nanomaterial definitions and safety evaluation considerations. *Regul. Toxicol. Pharm.*, **2015**, *73*, 137-150

(*26*) European Commission. Environment. Chemicals. Definition of nanomaterial. https://ec.europa.eu/environment/chemicals/nanotech/faq/definition_en.htm (accessed May 07, 2020)

(*27*) Khan, I.; Saeed, K.; Khan, I. Nanoparticles: properties, applications, and toxicities. *Arab. J. Chem.*, **2019**, *12*, 908-931

(*28*) Shang, L.; Dong, S.; Nienhaus, G. U. Ultra-small fluorescent metal nanoclusters: synthesis and biological applications. *Nano Today*, **2011**, *6*, 401-418

(*29*) Casadei, A.; Pecora, E. F.; Trevino, J.; Forestiere, C.; Rüffer, D.; Averchi, E. R.; Matteini, F.; Tutuncuoglu, G.; Heiss, M.; i Morral, A. F.; Negro, L. D. Photonic-plasmonic coupling of GaAs single nanowires to optical nanoantennas. *Nano Lett.*, **2014**, *14* (5), 2271-2278

(*30*) Ekimov, A. I.; Onushchenko, A. A.; Quantum size effect in three-dimensional microscopic semiconductor crystals. *JETP Lett.*, **1981**, *34* (6), 345-349

(*31*) Alivisatos, A. P. Semiconductor clusters, nanocrystals, and Quantum Dots. *Science*, **1996**, *271* (5251), 933-937

(*32*) Suárez, P. L.; Cortes, M. G.; Argüelles, M. T. F.; Encinar, J. R.; Valledor, M.; Ferrero, F. J.; Campo, J. C.; Fernández, J. M. C. Functionalized phosphorescent nanoparticles in (bio)chemical sensing and imaging – A review. *Anal. Chim. Acta*, **2019**, *1046*, 16-31

(*33*) Yang, J.; Ling, T.; Wu, W. T.; Liu, H.; Gao, M. R.; Ling, C.; Li, L.; Du, X. W. A top-down strategy towards monodisperse colloidal lead sulphide Quantum Dots. *Nat. Commun.*, **2013**, *4*, 1695

(*34*) Speranskaya, E. S.; Beloglazova, N. V.; Abe, S.; Aubert, T.; Smet, P. F.; Poelman, D.; Goryacheva, I.; Saeger, S. D.; Hens, Z. Hydrophilic, bright $CuInS_2$ Quantum Dots as Cd-free fluorescent labels in quantitative immunoassay. *Langmuir*, **2014**, *30* (25), 7567-7575

(*35*) Chen, S.; Imoukhuede, P. I. Multiplexing angiogenic receptor quantification via Quantum Dots. *Anal. Chem.*, **2019**, *91*, 7603-7612

(*36*) González, E. S.; Roces, L.; Granda, S. G.; Argüelles, M. T. F.; Fernández, J. M. M.; Medel, A. S. Influence of Mn^{2+} concentration on Mn^{2+}-doped ZnS Quantum Dot synthesis: evaluation of the structural and photoluminescent properties. *Nanoscale*, **2013**, *5*, 9156-9161

(*37*) Chen, H. Y.; Chen, T. Y.; Son, D. H. Measurement of energy transfer time in colloidal Mn-doped semiconductor nanocrystals. *J. Phys. Chem. C*, **2010**, *114* (10), 4418-4423

(*38*) Bhargava, R. N.; Gallagher, D.; Hong, X.; Nurmikko, A. Optical properties of manganese-doped nanocrystals of ZnS. *Phys. Rev. Lett.*, **1994**, *72* (3), 416-419

(*39*) García-Cortés, M.; González, E. S.; Argüelles, M. T. F.; Encinar, J. R.; Fernández, J. M. C.; Medel, A. S. Capping of Mn-doped ZnS Quantum Dots with DHLA for their stabilization in aqueous media: determination of the nanoparticle number concentration and surface ligand density. *Langmuir*, **2017**, *33*, 6333–6341

(*40*) Montaño, M. D.; Olesik, J. W.; Barber, A. G. Single particle ICP_MS: advances toward routine analysis of nanomaterials. *Anal. Bioanal. Chem.*, **2016**, *408*, 5053-5074

(*41*) Pace, H. E.; Rogers, N. J.; Jarolimek, C.; Coleman, V. A.; Higgins, C. P.; Ranville, J. F. Determining transport efficiency for the purpose of counting and sizing nanoparticles

via single particle inductively coupled plasma mass spectrometry. *Anal. Chem.,* **2011**, *83* (24), 9361-9369

(*42*) Liu, X.; Braun, G. B.; Qin, M.; Rosulate, E.; Sugahara, K. N. In vivo cation exchange in Quantum Dots for tumor-specific imaging. *Nat. Commun.*, **2017**, *343*

(*43*) Wang, Y.; Wang, P.; Wu, Y.; Di, J. A cathodic "signal-on" photoelectrochemical sensor for Hg^{2+} detection based on ion-exchange with ZnS Quantum Dots. *Sensor. Actuat. B-Chem.*, **2018**, *254*, 910-915

(*44*) Jacob, J. M.; Rajan, R.; Aji, M.; Kurup, G. G.; Pugazhendhi, A. Bio-inspired ZnS Quantum Dots as efficient photo catalysts for the degradation of methylene blue in aqueous phase. *Ceram. Int.*, **2019**, *45*, 4857-4862

(*45*) Lu, Z.; Chen, X.; Wang, Y.; Zheng, X.; Li, C. M. Aptamer based fluorescence recovery assay for aflatoxin B1 using a quencher system composed of Quantum Dots and graphene oxide. *Microchim. Acta*, **2015**, *182*, 571-578

(*46*) Dos Santos, M. C.; Algar, W. R.; Medintz, I. L.; Hildebrandt, N. Quantum Dots for Förster Resonance Energy Transfer (FRET). *TrAC-Trend. Anal. Chem.*, **2020**, *125*

(*47*) Bell, A.; Wang, Z. J.; Ghahroudi, M. A.; Chang, T. A.; Durocher, Y.; Trojahn, U.; Baardsnes, J.; Jaramillo, M. L.; Li, S.; Baral, T. N.; McCourt, M. O.; MacKenzie, R.; Zhang, J. Differential tumor-targeting abilities of three single-domain antibody formats. *Cancer Lett.*, **2010**, *289*, 81-90

(*48*) Vashist, S. K.; Schneider, E. M.; Luong, J. H. T. Surface plasmon resonance-based immunoassay for human C-reactive protein. *Analyst*, **2015**, *140* (13), 4445-4452

(*49*) Liu, B.; Zhang, B.; Chen, G.; Tang, D. Biotin-avidin-conjugated metal sulfide nanoclusters for simultaneous electrochemical immunoassay of tetracycline and chloramphenicol. *Microchim. Acta*, **2014**, *181*, 257-262

(*50*) Haugland, R. P.; You, W. W. Coupling of antibodies with biotin, In *Avidin-biotin interactions. Methods in molecular biology*; McMahon, R. J., Eds.; Humana Press: Totowa, NJ, 2008; Vol. 418, pp 13-14

(*51*) Tan, Y. H.; Liu, M.; Nolting, B.; Go, J. G.; Hague, J. G.; Liu, G. Y. A nanoengineering approach for investigation and regulation of protein immobilization. *ACS Nano*, **2008**, *2* (11), 2374-2384

(*52*) Smith, A. M.; Nie, S. Semiconductor Quantum Dots for molecular and cellular imaging, In *Tissue engineering and artificial organs: The biomedical engineering handbook*, 3rd edition; Bronzino, J. D., Eds.; CRC Press: Hartford, CT, 2006; Vol. 3, pp 22-2

(*53*) González, E. S.; Argüelles, M. T. F.; Fernández, J. M. C.; Medel, A. S. Mn-doped ZnS Quantum Dots for the determination of acetone by phosphorescence attenuation. *Anal. Chim. Acta*, **2012**, *712*, 120-126

(*54*) Haynes, W. M. *Handbook of chemistry and physics*, 97th edition; CRC Press: Boca Raton, FL, 2017, pp 7,1-7,2

(*55*) Clapp, A. R.; Goldman, E. R.; Mattoussi, H. Capping of CdSe-ZnS Quantum Dots with DHLA and subsequent conjugation with proteins. *Nat. Protoc.*, **2006**, *1* (3), 1258-1266

(*56*) García-Cortés, Argüelles, M. T. F.; Fernández, J. M. C.; Medel, A. S. Sensitive prostate specific antigen quantification using dihydrolipoic acid surface-functionalized phosphorescent Quantum Dots. *Anal. Chim. Acta*, **2017**, *987*, 118-126

(*57*) Burdick, Lisa. Urine Drug Test HQ. https://urinedrugtesthq.com/how-to-make-synthetic-pee/ (accessed June 29, 2020)